



ELSEVIER

Contents lists available at [ScienceDirect](https://www.sciencedirect.com)

Mechanical Systems and Signal Processing

journal homepage: www.elsevier.com/locate/ymssp

Comparative performance assessment of methods for operational modal analysis during transient order excitation

German Sternharz^{a,*}, Tatiana Kalganova^a, Cristinel Mares^b, Moritz Meyeringh^c

^a Brunel University London, CEDPS, Department of Electronic and Computer Engineering, Kingston Lane, Uxbridge, Middlesex UB8 3PH, United Kingdom

^b Brunel University London, CEDPS, Department of Mechanical and Aerospace Engineering, Kingston Lane, Uxbridge, Middlesex UB8 3PH, United Kingdom

^c Rolls-Royce Deutschland Ltd & Co KG, Eschenweg 11, 15827 Blankenfelde-Mahlow, Germany

ARTICLE INFO

Keywords:

Operational modal analysis
Order-based modal analysis
Rotating machinery
Order tracking
Harmonic excitation
Monte-Carlo simulation

ABSTRACT

Machinery with rotating components poses a challenge to Operational Modal Analysis (OMA) due to its periodic inputs, i.e. orders. Transient (acceleration or deceleration) runs represent a relevant test condition for structures, which experience a low amount of broadband (noise) excitation during operation. In these cases, orders present themselves as a favourable source of excitation. However, this type of excitation can result in distortions of the response spectrum at the ending frequencies of individual orders. These “end-of-order” distortions can introduce spurious or biased modal estimations. Order-based Modal Analysis (OBMA) is an OMA method, which was developed specifically for the transient test case and is not affected by end-of-order distortions. However, some downsides are associated with OBMA because it performs modal analysis for each relevant order individually. In addition to the associated analysis effort, this produces multiple sets of modal estimations with ambiguous results. This paper introduces an extension of OBMA to address these issues. The proposed method, called Averaged Order-based Modal Analysis (AOBMA), applies scaling and (weighted) averaging to extracted orders prior to the modal estimation step. A Monte-Carlo simulation study is introduced to compare the modal estimation performance of traditional OMA, OBMA and AOBMA. Different ratios of harmonic and random excitation amplitudes are simulated to gauge the impact of the excitation’s composition. In addition, all methods are also applied to operational measurements from a turbofan casing during run-up. The results indicate that AOBMA produces a lower variance in the estimated modal parameters compared to OBMA. Moreover, while OMA was more successful in the estimation of closely spaced modes, it was surpassed by AOBMA and OBMA regarding the accuracy of mode shape estimations.

1. Introduction

Accurate knowledge of modal parameters is often required for both the design and evaluation of engineering structures. As a foundation for reduction of noise and vibration, the risk of damage can be reduced, and maintenance intervals optimised. Another common application of modal parameters is the validation and optimisation of Finite Element Method (FEM) models by model

* Corresponding author.

E-mail address: german.sternharz@brunel.ac.uk (G. Sternharz).

<https://doi.org/10.1016/j.ymssp.2021.108719>

Received 12 July 2021; Received in revised form 1 December 2021; Accepted 1 December 2021

Available online 31 December 2021

0888-3270/© 2021 The Authors.

Published by Elsevier Ltd. This is an open access article under the CC BY license

(<http://creativecommons.org/licenses/by/4.0/>).

updating.

Operational Modal Analysis (OMA) can be used to estimate these modal parameters. In contrast to Experimental Modal Analysis (EMA), OMA does not require the knowledge or measurement of the input forces and thus can be applied to structures, which are excited by operational or environmental forces. Benefits of this approach are that complex and large structures (which may not be suitable for EMA) can be tested under realistic operating (incl. boundary and forcing) conditions, producing correspondingly representative results.

Rotating components in operating structures have a characteristic excitation due to unbalance and other periodic disturbances. The instantaneous rotation rate represents the foundational frequency and is typically superimposed with higher harmonics. These periodic input forces are also known as orders. However, OMA usually relies on the assumption of uncorrelated input forces with zero mean and a flat spectrum (i.e. the characteristics of white noise) [1]. Deviations from this assumption can lead to false or biased modal estimations [2–4], thus making results of OMA more challenging to interpret. This is not only true for rotating machinery at stationary operating conditions, where the input orders result in narrow-banded peaks in the force spectrum but also for transient (acceleration or deceleration) runs, which produce so-called end-of-order distortions, as will be shown later in Section 2.3.

Several approaches to address this issue and to facilitate OMA of structures with rotating components is available in the literature and a survey is provided, for example, in [5]. This includes methods for pre-processing, which aim to reduce harmonic peaks from the measured output signal; adapted OMA methods, which require explicit information of disturbing harmonics; and OMA methods, which implicitly consider harmonics or are not negatively affected by them.

A method from the latter category is Order-based Modal Analysis (OBMA). It relies on order excitation and uses order tracking to supply extracted orders as the data foundation for OMA. Most methods and studies consider the case of (approximately) stationary operation, while the analysis of rotating machinery at transient (i.e. acceleration or deceleration) operating conditions is a less researched field. However, in test cases where broadband forces during operation are too low for sufficient excitation of modes, transient runs with order excitation can lead to a more complete modal estimation [6]. OBMA is specifically developed for measurement data from transient runs and has the benefit that it is free of spurious end-of-order modes, which can be falsely identified by common OMA methods [7–9].

A survey of existing case studies of OBMA is a previous work of the authors of this paper and it considered the amount of periodic and random excitation [6]. However, the potential impact of the force composition was not explicitly considered by existing previous studies, which hinders conclusions on this question. The present paper addresses this gap by systematically analysing simulation response data with varying ratios of harmonic and random excitation amplitudes. The potential impact of the excitation force composition is a relevant research question since it is test case specific and could determine suitable data processing or analysis methods. For example, a single turbofan component, which is driven by an electromagnetic motor in a laboratory spinning test will likely experience a greater order excitation and a lower degree of operational random forces compared to a turbofan engine under operational and environmental forces in flight.

It was also found that there is limited literature, which quantifies the modal estimation performance of OBMA in comparison to alternative, traditional OMA methods [6]. For example, just a single case study was found, which provided a comparison of mode shape estimations between OBMA and OMA using the Modal Assurance Criterion (MAC) [10]. Multiple studies observed OBMA partially resulting in high overestimation errors of damping ratios, especially in the case of lightly damped modes [9–12]. Since OBMA processes tracked orders individually, each processed order of a dynamic structure provides a separate set of modal estimations. These sets of results can vary notably from one order to another [10], increasing the effort in analysis and result interpretation.

This paper addresses the stated issues and provides the following contributions:

- The impact of the force composition (in terms of harmonic and random amplitudes) on modal estimation results is systematically analysed using a parametric Monte Carlo simulation study.
- The modal estimation accuracy of OBMA is evaluated in terms of deviations from simulation reference parameters as well as in comparison to a traditional OMA method using operational test measurements.
- A novel method and extension of OBMA, the Averaged Order-based Modal Analysis (AOBMA), is introduced, aiming to address the issue of separate result sets with partially great estimation error differences.
- For validation and performance assessment, AOBMA is applied alongside OBMA and a reference OMA method to response data from simulation data as well as operational data of a turbofan casing during acceleration.

Following this introductory section, this paper is structured as follows. First, Section 2 gives an overview of the compared modal analysis methods and the (Pole-weighted) Extended Modal Assurance Criterion (MACXP). It continues with specifics of order excitation, including end-of-order distortions, followed by the theory and implementation details of the novel AOBMA method. Next, the test setups for the used simulation and operational data are introduced along with the analysis methodology for validation and performance assessment of the compared modal estimation methods in Section 3. Section 4 covers the results from the parametric simulation study and the operational test measurements. Finally, conclusions and suggestions for future work are given in Section 5.

2. Theory

In the first subsection of this chapter, an overview and the relation of each of the compared OMA methods is given. Afterwards, the MACX and MACXP are introduced. These metrics extend the MAC to applications with complex modes and are used in the comparative analysis of modal estimation results in Section 4. The impact of order excitation on the measured response is investigated next,

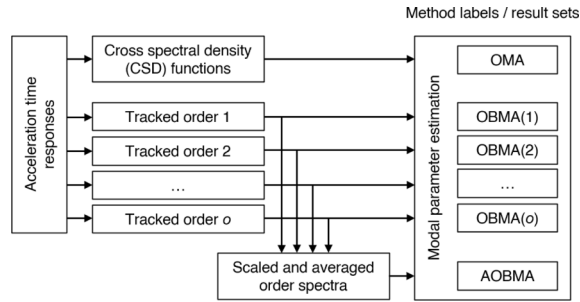


Fig. 1. Processing steps of the compared methods OMA, OBMA and AOBMA.

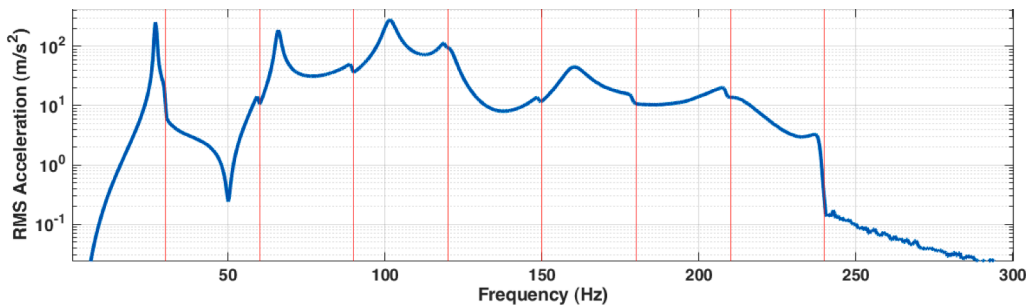


Fig. 2. Acceleration output spectrum of the simulated structure at node 1 (Fig. 11), X direction, harmonic ratio 0.8.

followed by the last subsection, which covers the theory and implementation details of AOBMA.

2.1. Overview of compared OMA methods

As the foundational OMA method, the Alias-Free Polyreference (AFPoly) method [15] is used in this study. This frequency-domain modal estimation method is based on the orthogonal rational fraction polynomial method (RFP) [16] and is implemented in the software MEScope. In comparison to RFP, AFPoly introduces a generalized companion matrix, which resolves the issue of ill-conditioning of modal models with high polynomial orders. Since the method operates in the Laplace domain, it has the benefit that the impact (i.e. aliasing) of out-of-band modes is avoided, resulting in less computational modes and clearer stabilisation diagrams. This is in contrast to other common OMA methods, which operate in the discrete-time domain or z-domain, including the (polyreference) Least-Squares Exponential (pLSCE) and Complex Frequency (pLSCF) methods [15,17]. The method is used hereafter in three configurations:

1. Cross-spectra-based Operational Modal Analysis (OMA)
2. Order-Based Modal Analysis (OBMA)
3. Averaged Order-Based Modal Analysis (AOBMA)

Each method is introduced further below and the relation between the methods is visualised in Fig. 1.

In a classical OMA application, Cross Spectral Densities (CSD) are calculated from the DOFs’ acceleration responses with the Welch’s method and are used as the inputs to the OMA method. As a common OMA procedure, this approach is simply denoted “OMA” in the following and acts as the reference method for this study.

For OBMA, individual order functions are extracted from the acceleration response at each DOF by order tracking. The requirements are that a tachometer signal is available to provide the rotations per minute (rpm) and that an acceleration or deceleration run of the operating machine is measured, where the extracted orders cover a desired frequency range for later analysis. For the present paper, order tracking is performed using resampling to the angle-domain (AD). This method was compared with other order tracking algorithms for the specific use with OBMA before and provided satisfying results [18,19]. For more constrained test conditions, e.g. with the presence of crossing orders, alternative methods are available, including the Time Variant Discrete Fourier Transform (TVDFFT) and Vold-Kalman (VK) order tracking. In the AD method, angular resampling of the original time-domain data provides order-synchronous signals. Afterwards, the Fourier transform is applied to obtain order-domain spectra, which are assembled into an order-rpm spectrogram. In this spectrogram, each row represents an order as a function of rpm, so the orders of interests are easily extracted. A frequency-domain response is estimated by converting the rpm axis values to the instantaneous frequencies of the *l*-th order using the relationship in Eq. (1). Finally, each of the extracted orders is processed by a modal estimation algorithm individually,

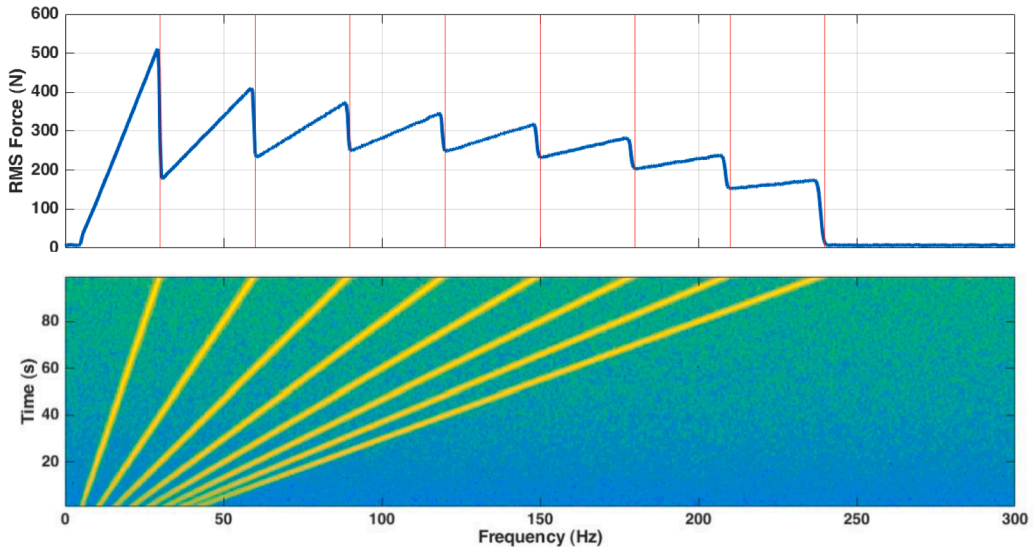


Fig. 3. Force input spectrum (top) and spectrogram (bottom) of the simulated structure.

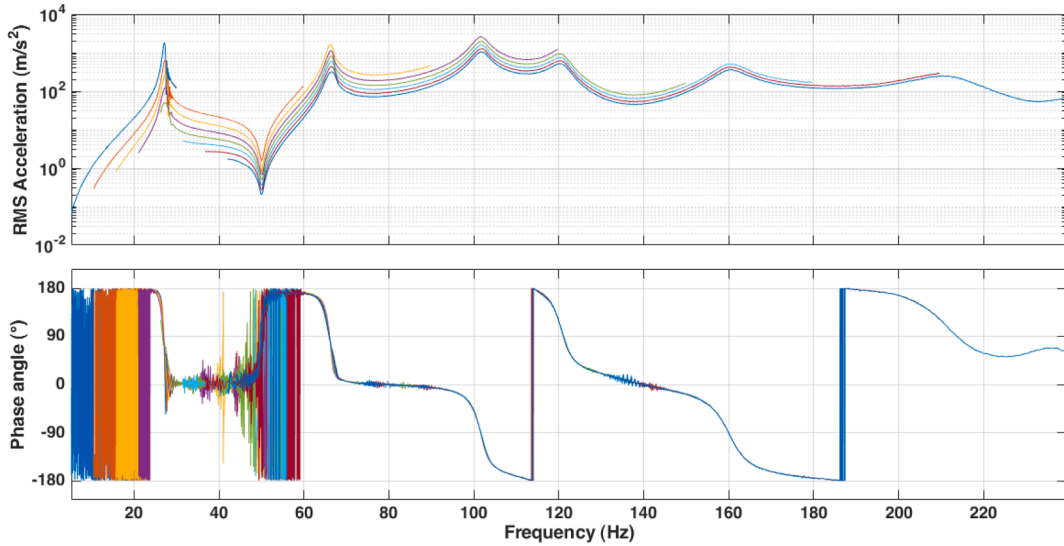


Fig. 4. Individual extracted response orders.

resulting in a set of estimated modal parameters per order.

$$f_i = (l \text{ rpm})/60 \tag{1}$$

AOBMA is based on the same steps as OBMA with the addition that the extracted orders are averaged into a single spectrum before applying modal estimation. To avoid discontinuities between orders without splitting the extracted orders to smaller sections (more on this in Section 2.4), the averaged orders should have similar magnitudes across their combined frequency range. Since the order amplitudes generally are not similar, the orders are first scaled by calculating the relative amplitude differences between subsequent orders. These difference functions are then used to detrend individual orders to a common level before a (weighted) averaging of the orders is applied. AOBMA is explained in more detail in Section 2.4.

2.2. Extended Modal Assurance Criterion

The Modal Assurance Criterion (MAC) [20] is a common metric to quantify the consistency between two mode shape vectors $\{v_1\}$ and $\{v_2\}$. The MAC can be calculated by Eq. (2), where \bullet^H denotes a complex conjugate transpose (i.e. Hermitian).

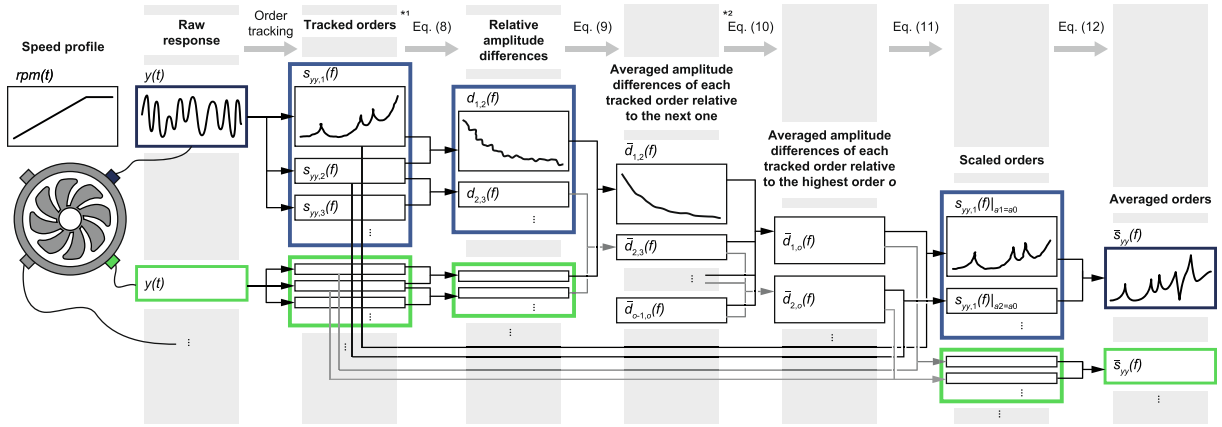


Fig. 5. Procedural diagram of AOBMA; additional steps covered in Section 2.4.1: *¹ prior to Eq. (7), interpolation of tracked orders to common frequency values; *² prior to Eq. (9), smoothing (e.g. moving average) due to order spectrum distortions.

$$MAC(\{v_1\}, \{v_2\}) = \frac{|\langle v_1^H \rangle \{v_2\}|^2}{\langle v_1^H \rangle \{v_1\} \langle v_2^H \rangle \{v_2\}} \tag{2}$$

The MAC is well suited for modes shapes, where the individual vector components form a straight line in the complex plane [13]. Such mode shapes are called monophasic or are said to have a low degree of complexity or a high Modal Phase Collinearity (MPC) close to 1. However, for the general case of non-proportional damping in combination with close or repeated modes, this condition is not satisfied [21]. In such cases, the MAC value is not conclusive. The Extended Modal Assurance Criterion (MACX) [13] is a generalisation of the MAC and addresses its potential issues when applied to complex mode shapes. The MACX is defined by Eq. (3), where •^T is the transpose operation.

$$MACX(\{v_1\}, \{v_2\}) = \frac{(|\langle v_1^H \rangle \{v_2\}| + |\langle v_1^T \rangle \{v_2\}|)^2}{(\langle v_1^H \rangle \{v_1\} + |\langle v_1^T \rangle \{v_1\}|)(\langle v_2^H \rangle \{v_2\} + |\langle v_2^T \rangle \{v_2\}|)} \tag{3}$$

A further extension of MACX is the Pole-weighted MACX (MACXP). It can be considered as the application of the MACX to vectors {V₁} and {V₂}, which contain the free decay time series of individual DOFs with the natural frequency and damping ratio corresponding to the pole λ₁ and λ₂, respectively. By evaluating the limits of the time interval Δt and number of time samples n_r in the free decays, the following equation can be constructed for MACXP [13], where •* is the complex conjugate:

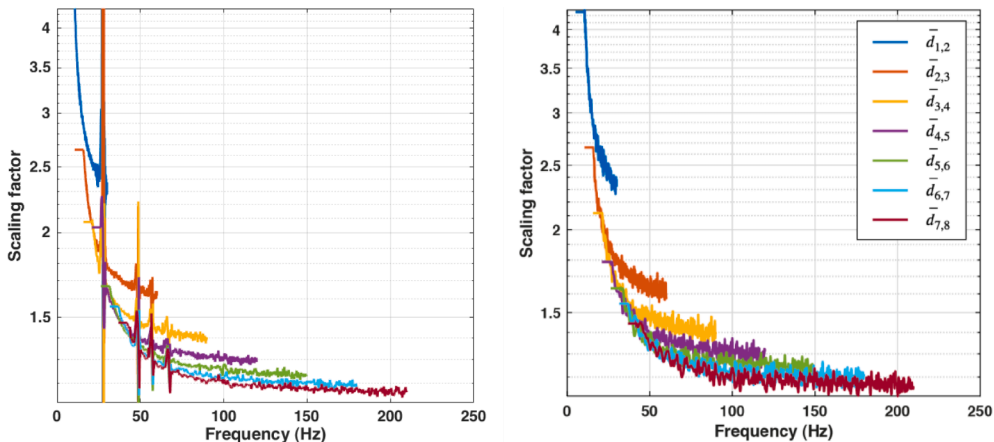


Fig. 6. Averaged difference functions d̄_{l,l+1} of subsequent orders based on order output acceleration (left) and order input force (right).

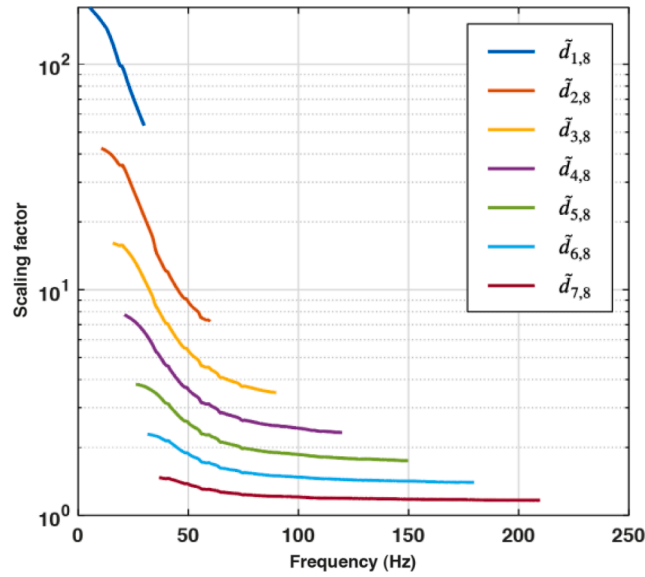


Fig. 7. Trend functions $\tilde{d}_{l,o}$ from each order l to the highest order $o = 8$.

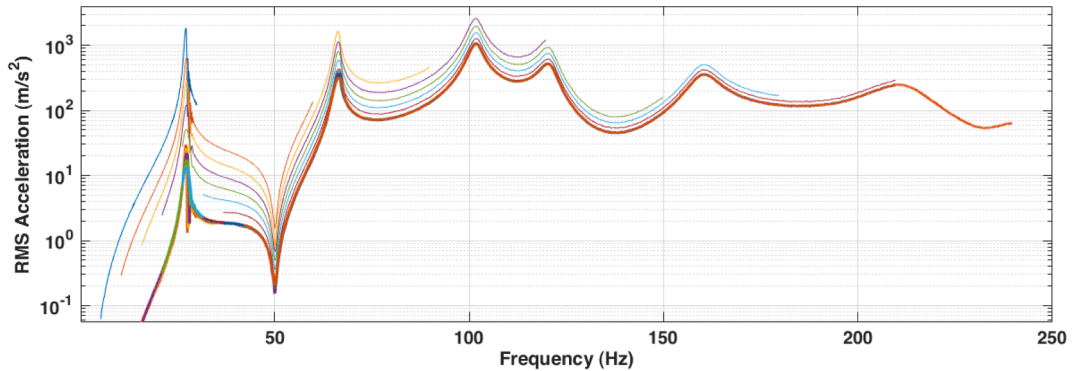


Fig. 8. Individual order magnitudes before scaling (light lines) and after scaling (bold lines).

$$MACXP(\{v_1\}, \{v_2\}) = \lim_{\substack{\Delta t \rightarrow 0 \\ n_f \rightarrow \infty}} MACX(\{V_1\}, \{V_2\}) = \frac{\left(\frac{|\langle v_1^H \rangle \{v_2\}|}{|\lambda_1^* + \lambda_2|} + \frac{|\langle v_2^H \rangle \{v_2\}|}{|\lambda_1 + \lambda_2|} \right)^2}{\left(\frac{|\langle v_1^H \rangle \{v_1\}|}{2|\operatorname{Re}(\lambda_1)|} + \frac{|\langle v_1^H \rangle \{v_1\}|}{2|\lambda_1|} \right) \left(\frac{|\langle v_2^H \rangle \{v_2\}|}{2|\operatorname{Re}(\lambda_2)|} + \frac{|\langle v_2^H \rangle \{v_2\}|}{2|\lambda_2|} \right)} \tag{4}$$

The MACX provides a consistent comparison of mode shape vectors with any type of complexity. The MACXP considers eigen-frequencies and damping ratios in addition to the mode shapes during the comparison of two modes. It is therefore used for matching of modes from different estimations in this paper. Furthermore, MACXP is significantly less sensitive to a low spatial resolution compared to MAC or MACX, allowing to distinguish modes with a lower number of measurement locations [13].

2.3. Characteristics of input and output spectra resulting from order excitation

This section uses data from the simulation setup, described in detail later in Section 3.1, to illustrate the impact of harmonic order excitation on the response spectrum and to discuss the end-of-order effect.

For modal identification with the reference OMA method, auto and cross-spectra are estimated from the time response using Welch’s method. The linear auto-spectrum in Fig. 2 shows discontinuities at the frequencies, where individual orders end (marked with vertical red lines). They are due to the end-of-order effect but can be misinterpreted as the system response and can thus lead to falsely identified modes [7–9].

The origin of this phenomenon becomes clear when visualising the spectrum and spectrogram of the input force in Fig. 3.

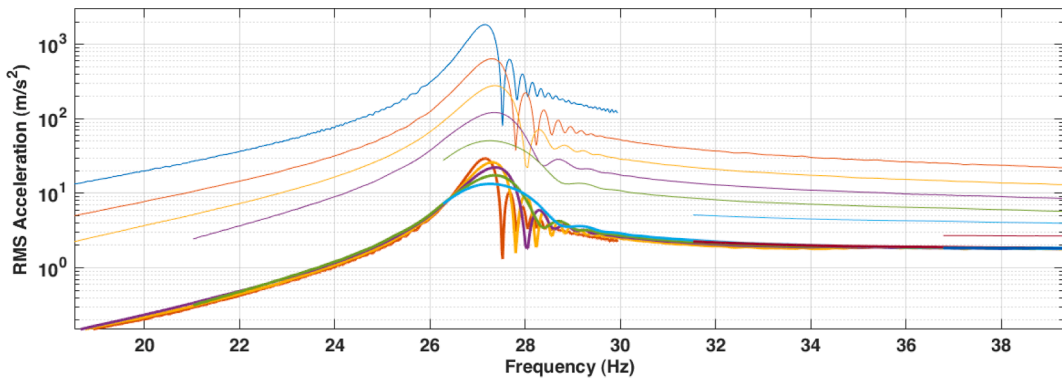


Fig. 9. Individual order magnitudes before scaling (light lines) and after scaling (bold lines) around the first resonance.

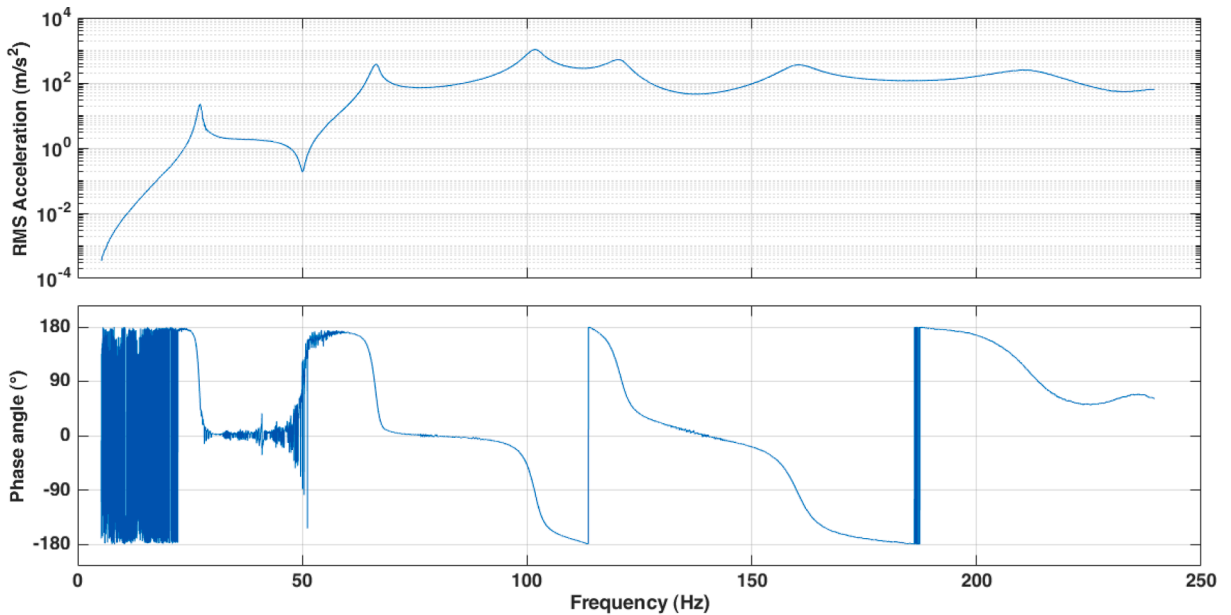


Fig. 10. Resulting response signal after order scaling and averaging with AOBMA.

The input orders can be regarded as an excitation by multiple simultaneous sweeps with different sweeping rates. The underlying individual orders with linearly increasing amplitudes (defined in Eq. (13)) are visible in the input spectrum plot. A sawtooth pattern is formed due to the abrupt ending of the individual orders' contribution to the excitation. This strong deviation from a flat input spectrum is reflected in the output spectrum in Fig. 2. The greatest distortion in Fig. 3 (top) is visible at the frequency range of the first order, which shows the highest amplitude slope as well as the greatest abrupt decrease at its end. This trend decreases with higher orders.

This progression can be attributed to two factors:

1. Increasing frequency bandwidths (i.e. decreasing sweeping rates) of increasing orders result in lower spectral amplitudes. The reason is that the Fourier transform of a sweep is proportional to $\sqrt{T/(2W)}$, where T is the total sweep duration and W is the frequency bandwidth of the sweep. This has been shown for sweeps with a linear frequency function and constant amplitude [14].
2. The rows of the spectrogram in Fig. 3 can be considered as colour-coded spectra of (overlapping) time blocks of the original signal. The averaging of these individual spectra represents Welch's method, which estimates the overall spectrum shown in the top portion of Fig. 3. When multiple orders cover a certain frequency range, they all contribute to the resulting average (i.e. the estimated spectrum amplitude) in this range. At rising frequencies, less and less orders are present in the excitation, leading to the smallest spectrogram amplitudes above 210 Hz, where solely the last order is contributing to the excitation.

It was observed that higher harmonic ratios (i.e. greater order amplitudes with a steeper increase over rpm) produce stronger end-

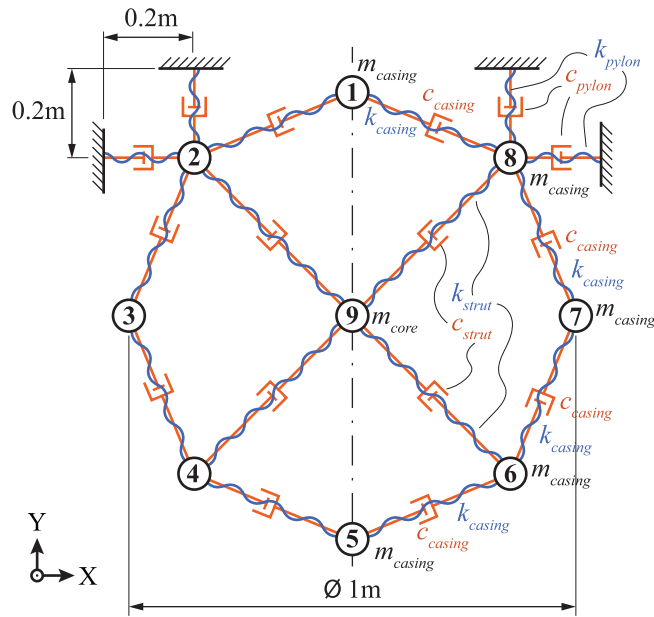


Fig. 11. Definition of the geometry and element types of the simulated dynamic structure.

Table 1
Simulation parameters.

Mechanical properties	
Masses: $m_{core} = 10$ kg, $m_{casing} = 1$ kg	
Stiffnesses: $k_{casing} = 500000$ N/m, $k_{pylon} = 1e + 6$ N/m, $k_{strut} = 500000$ N/m	
Damping coefficients: $c_{casing} = 20$ Ns/m, $c_{pylon} = 50$ Ns/m, $c_{strut} = 30$ Ns/m	
Time response simulation	
Linear acceleration Newmark (implicit) time integration method	
Simulation sampling frequency: $f_s = 5$ kHz	

Table 2
Reference values for eigenfrequencies and damping ratios of the simulated structure.

Mode	Natural frequency f_{ref} [Hz]	Damping ratio ξ_{ref}	Mode	Natural frequency f_{ref} [Hz]	Damping ratio ξ_{ref}
1	0.00	0.00%	10	120.56	1.75%
2	0.00	0.00%	11	138.70	2.24%
3	26.37	0.47%	12	160.25	2.28%
4	26.85	0.48%	13	177.05	2.30%
5	47.40	0.67%	14	198.82	2.60%
6	55.96	0.77%	15	207.42	3.35%
7	65.94	0.93%	16	212.39	3.28%
8	97.70	1.43%	17	229.57	3.18%
9	101.53	1.69%	18	239.84	3.27%

of-order distortions. In addition, the effect appears to be more pronounced when a higher number of spectrum averages is used in the Welch’s method.

By applying order tracking to the output signal, individual response orders can be extracted, which are shown in Fig. 4. It is visible, that the individual orders are free of discontinuities present in Fig. 2. This fact is utilised by the OBMA method, which performs OMA based on individual orders. However, this leads to multiple sets of modal results with overlapping frequency ranges, which can aggravate the interpretation of the results.

A possible solution to this limitation as well as an approach to reduce uncorrelated noise is to average the extracted orders into a single signal, which is the foundation of the proposed AOBMA method.

2.4. Order scaling and averaging in the AOBMA method

This section sets the theoretical foundation for the introduced AOBMA method. To supplement the theoretical descriptions, the subsequent Section 2.4.1 illustrates and discusses the application steps of the proposed method in practice based on simulated run-up

Table 3
Stabilisation criteria for modal identification.

Stabilisation criterion	Used value, (tested range)
Frequency tolerance (Hz)	0.2 (0.2...0.3)
Damping ratio tolerance (%)	1.5 (0.5...2)
Maximum model order	25
Minimum number of stable poles within the frequency and damping tolerances	4

Table 4
Tolerance criteria for matched mode estimations.

Tolerance quantity	Lower bound (incl.)	Upper bound (incl.)
Relative eigenfrequency error ($f_{est} - f_{ref}$)/ f_{ref}	-1%	1%
MACX (Eq. (3))	0.6	1

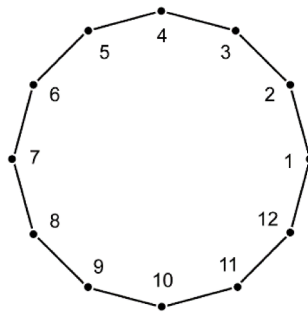


Fig. 12. Positions of accelerometers at the instrumented fan casing.

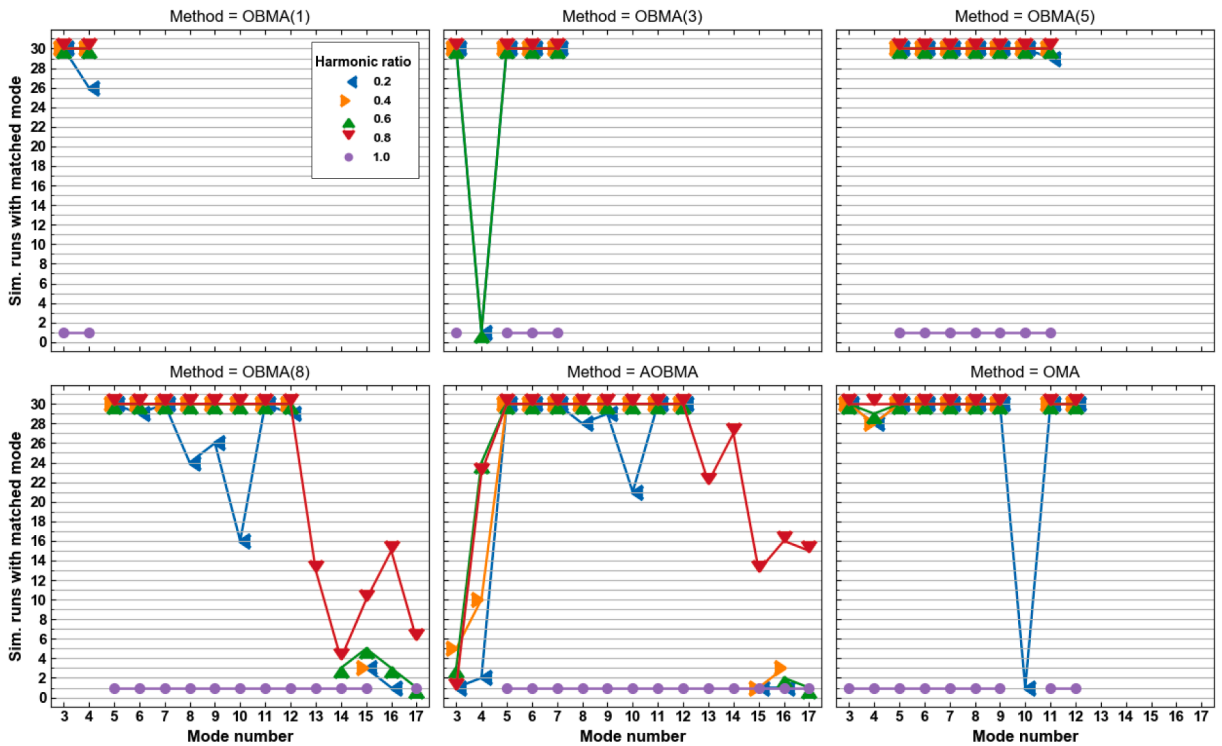


Fig. 13. Count of simulation runs with a matched estimation of the reference mode. For OBMA results, the individual source orders (1, 3, 5, 8) are specified in brackets.

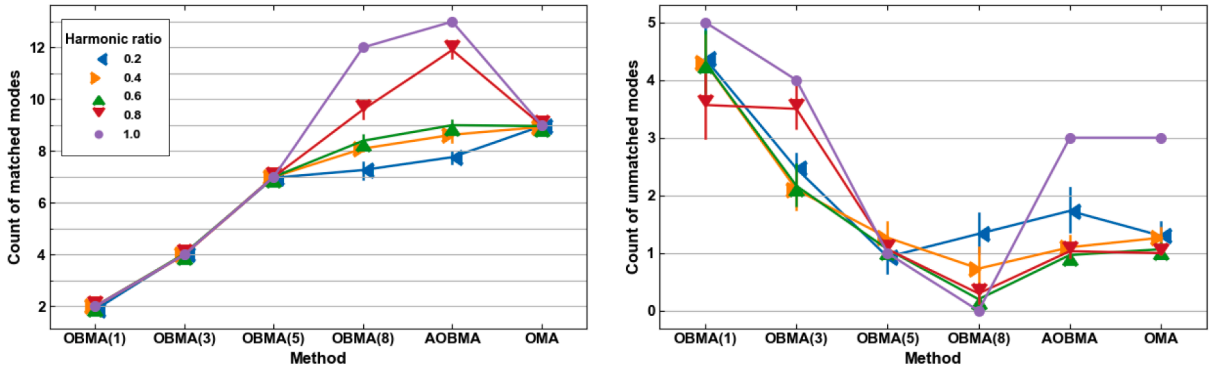


Fig. 14. Average count of matched (left) and unmatched (right) modes per single simulation run.

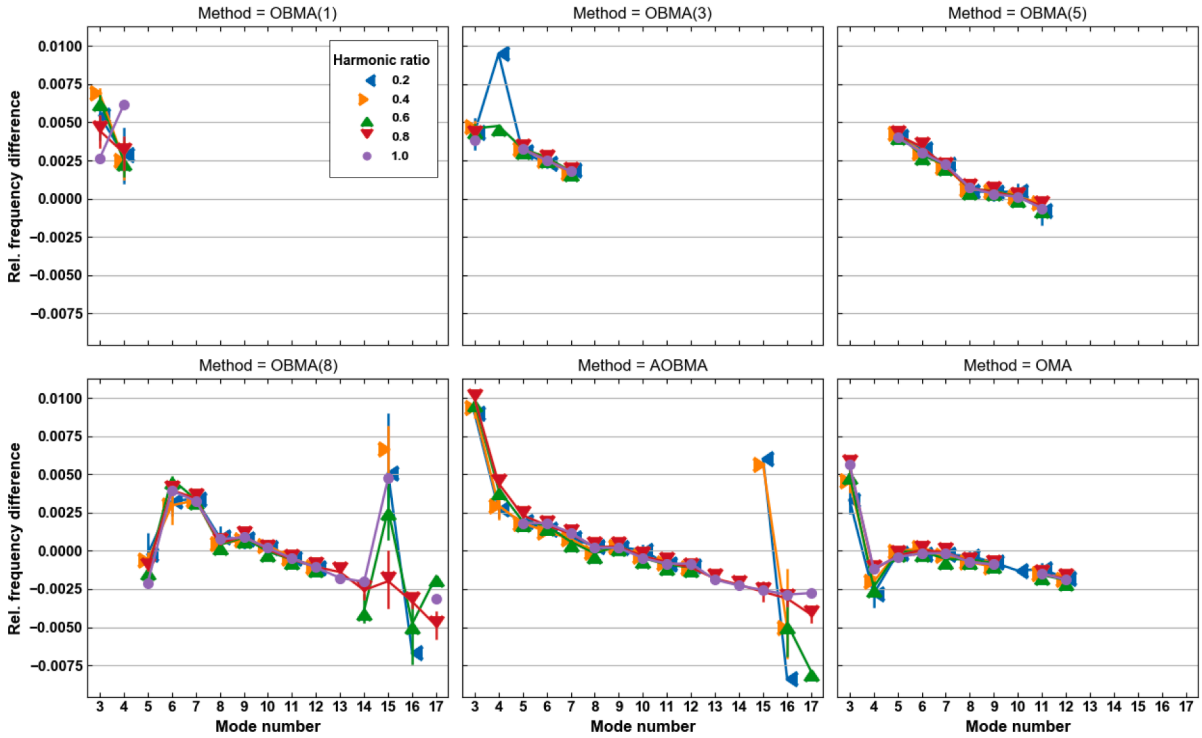


Fig. 15. Relative eigenfrequency errors $(f_{est} - f_{ref})/f_{ref}$ of matched mode estimations by different methods for individual harmonic ratios, where f_{est} and f_{ref} are the estimated and reference eigenfrequencies, respectively.

response data. Fig. 5 gives an overview of the processing steps and illustrates the data flow of AOBMA with references to the corresponding equations, which are presented in the course of this section.

Order averaging is not possible in a straightforward manner. Since the orders cover different frequency ranges and generally have different amplitudes, an average without further processing would suffer from similar discontinuities as the original output spectrum (Fig. 2). Previously, this issue has been addressed by subdividing the orders into frequency sections, where no contributing order begins or ends [7]. The downside of this approach is that either certain orders must be excluded from the averaging or the resulting sections would become impracticably small for modal analysis. As an alternative, the present work introduces an order scaling step prior to averaging, as described below. This allows averaging of all selected orders over their combined frequency range.

A tracked response order of a structure can be represented as a complex function of the excitation order frequency. This function is an estimate of the system response spectrum to an individual excitation order at a specific measurement location or DOF. For an order l , these response spectra can be constructed into an $(N \times N)$ spectral matrix $[S_{yy,l}]$, where the diagonal entries represent the auto-spectra of individual DOFs and the off-diagonal entries are the cross-spectra between DOFs.

By considering the relation between the frequency-domain force input and response output of the structure, which is given by the Frequency Response Function (FRF) matrix $[H]$, the relation between input and output spectrum matrices is obtained as [22]:

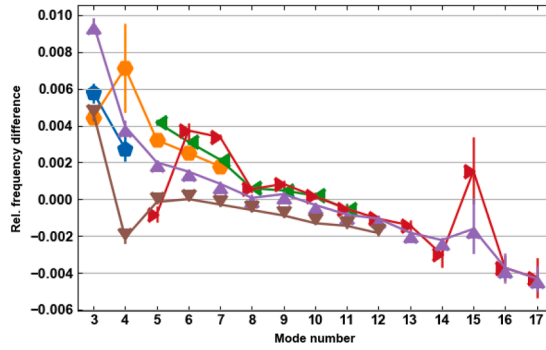


Fig. 16. Relative eigenfrequency errors of matched mode estimations by different methods (for the legend refer to Fig. 17).

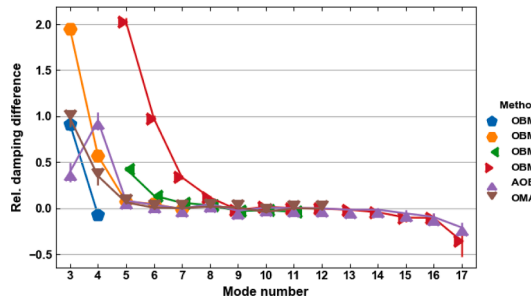


Fig. 17. Relative damping ratio errors $(\xi_{est} - \xi_{ref})/\xi_{ref}$ of matched mode estimations by different methods, where ξ_{est} and ξ_{ref} are the estimated and reference damping ratios, respectively.

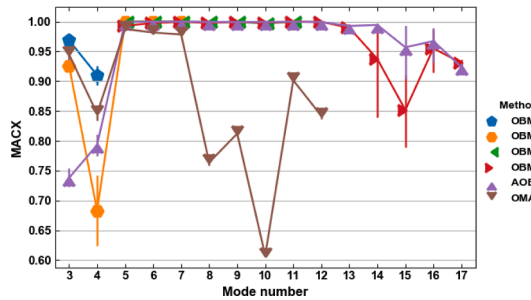


Fig. 18. MACX values of matched mode estimations by different methods.

$$[S_{yy,l}(f)] = [H(f)]^* [S_{xx,l}(f)] [H(f)]^T \tag{5}$$

where $[S_{yy,l}]$ is the spectral response matrix due to the excitation of a single order l described by the spectral input matrix $[S_{xx,l}]$.

The rotating input force of an order acts as a sinusoidal signal with a 90° (i.e. $\pi/2$) phase shift between the DOFs in X and Y directions. For example, in case of the simulated structure from upcoming Section 3.1, this force is applied to the central node 9 (Fig. 11). Assuming that these DOFs occupy the first 2 diagonal entries of $[S_{xx,l}]$, it can thus be written as:

$$[S_{xx,l}(f)] = a_l(f) \begin{bmatrix} 1 & e^{j\frac{\pi}{2}} & 0 & \dots \\ e^{j\left(-\frac{\pi}{2}\right)} & 1 & 0 & \dots \\ 0 & 0 & 0 & \dots \\ \vdots & \vdots & \vdots & \ddots \end{bmatrix} = a_l(f)[S_{xx}(f)] \tag{6}$$

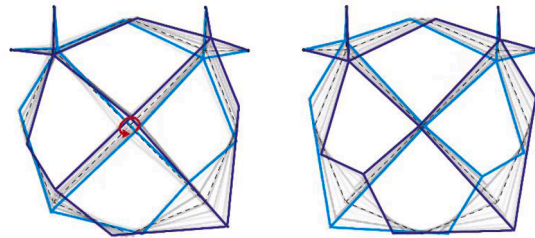


Fig. 19. Overlaid deflections of mode 12 estimated at harmonic ratio 0.8 by OMA (left) and AOBMA (right), dashed lines show the undeflected state, red arrow follows the trace of the central node (left).

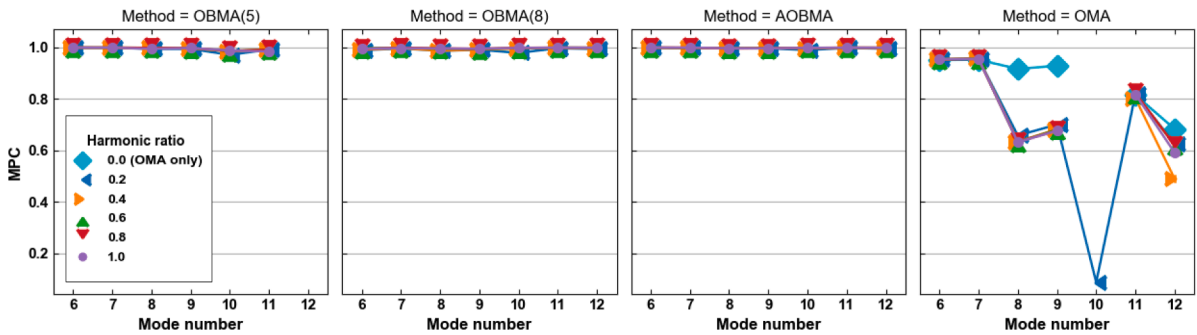


Fig. 20. MPC of mode shape estimations by different methods for individual harmonic ratios.

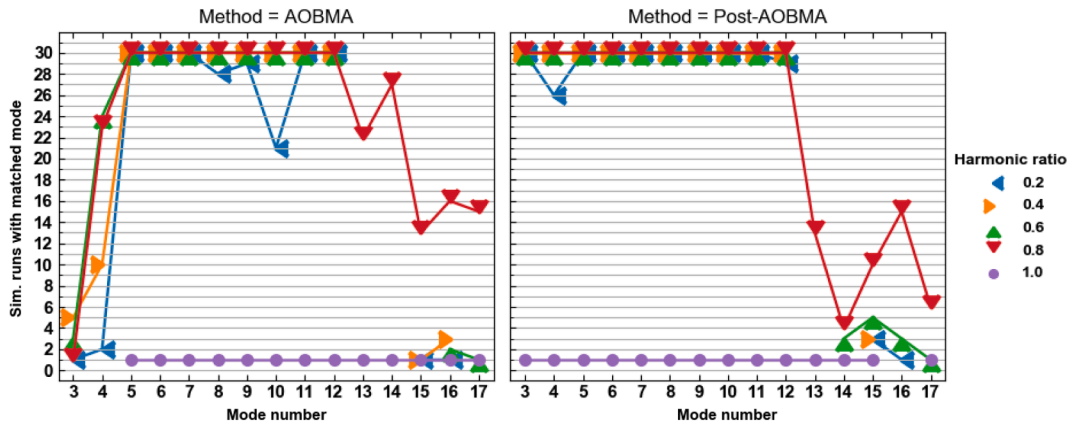


Fig. 21. Count of simulation runs with a matched mode estimation by AOBMA and Post-AOBMA.

where j is the imaginary number and $a_l(f)$ is the spectrum amplitude, which determines the frequency range covered by order l and the frequency-dependent input colouration, e.g. due to the linear amplitude increase like in the presented simulation.

Both the colouration of the input spectrum and the correlated excitation in X and Y directions (manifested in the off-diagonal terms of $[S_{xx,l}]$ in Eq. (6)) oppose the assumption of uncorrelated white noise in common OMA theory. The impact of these characteristics of order excitation on the output spectrum with respect to the modal model has been derived in previous studies [8,10,23]. It is shown that a frequency-dependent proportionality term is introduced in the output and specific components of the modal model (namely the participation factors and upper and lower residuals) become complex. From that, it is concluded and demonstrated that modal identification methods, which estimate a common denominator (i.e. characteristic) polynomial (in contrast to partial fraction estimators), are suited for modal estimation from this type of output spectra [9,24].

Under the assumption that subsequent excitation orders have a similar force distribution described by $[S_{xx,l}]$, the main difference between the orders lies in the order spectrum amplitude $a_l(f)$. The description of $[S_{xx,l}]$ in Eq. (6) can be substituted into Eq. (5).

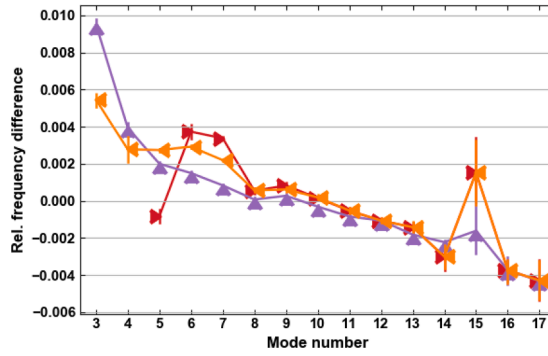


Fig. 22. Relative eigenfrequency errors of mode estimations by OBMA(8), AOBMA, Post-AOBMA (for the legend refer to Fig. 24).

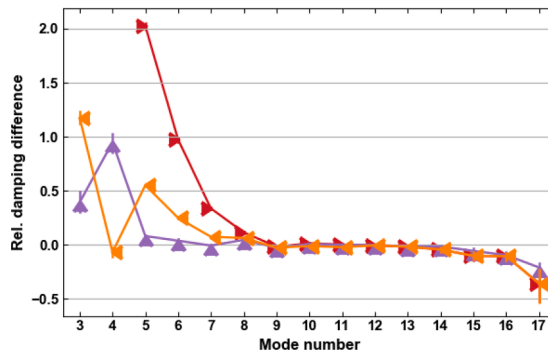


Fig. 23. Relative damping ratio errors of mode estimations by OBMA(8), AOBMA, Post-AOBMA (for the legend refer to Fig. 24).

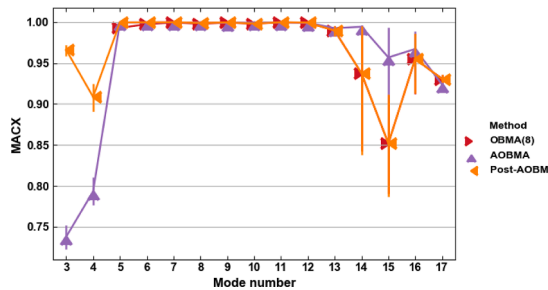


Fig. 24. MACX values of mode estimations by OBMA(8), AOBMA, Post-AOBMA.

Considering the elements of matrix $[S_{yy,l}]$, it becomes clear that the ratio of output spectra between subsequent orders l is driven by the relative difference between the input force amplitude $a_l(f)$ of subsequent orders:

$$\frac{s_{yy,l}^{(n,m)}(f)}{s_{yy,l+1}^{(n,m)}(f)} = \frac{a_l(f)}{a_{l+1}(f)} = d_{l,l+1}(f) \tag{7}$$

where $s_{yy,l}^{(n,m)}$ denotes the element of the output spectrum matrix $[S_{yy,l}]$ of order l at row n and column m . Thus, the relative amplitude difference $d_{l,l+1}$ can be estimated from the response spectrum at any DOF, provided that the response is present in the measurement locations, i.e. is not affected by a modal node in the frequency of interest. As shown by Eq. (7), the resulting ratio function $d_{l,l+1}$ is theoretically independent from the specific DOF or the element (n,m) of the output cross spectrum matrix. However, in practice the result will be influenced by errors due to measurements at nodal positions, nonlinear responses, measurement or processing methods

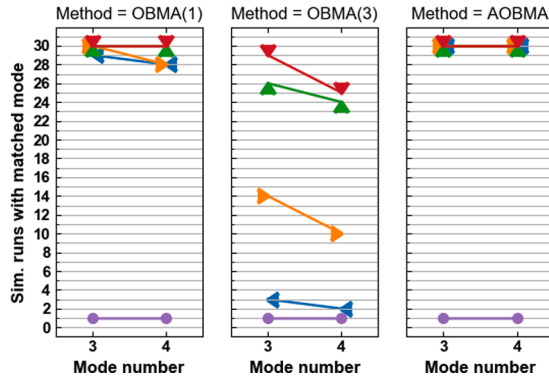


Fig. 25. Count of simulation runs with a matched mode, 25 Hz analysis bandwidth (for the legend refer to Fig. 26).

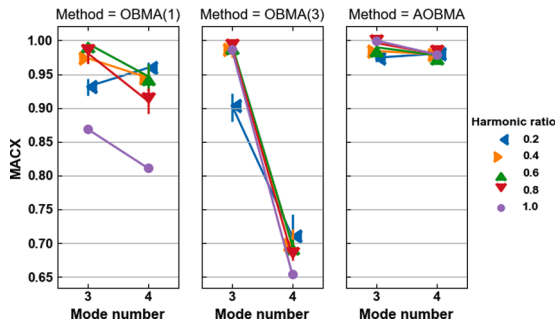


Fig. 26. MACX values of matched mode estimations, 25 Hz analysis bandwidth.

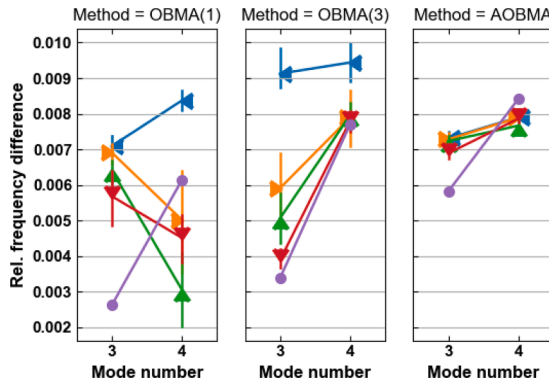


Fig. 27. Relative eigenfrequency errors of matched mode estimations, 25 Hz analysis bandwidth (for the legend refer to Fig. 26).

and the associated noise.

It is possible to reduce the uncorrelated errors and noise in $\hat{d}_{l,l+1}$ by calculating its values from different DOFs or elements (n,m) of the output spectrum matrix. Subsequent averaging of the individual estimates for $\hat{d}_{l,l+1}$ provides the averaged estimation $\bar{\hat{d}}_{l,l+1}$:

$$\bar{\hat{d}}_{l,l+1}(f) = \frac{1}{N} \sum_{n=1}^N \left(\frac{1}{N} \sum_{m=1}^N \frac{s_{yy,l}^{(n,m)}(f)}{s_{yy,l+1}^{(n,m)}(f)} \right) \tag{8}$$

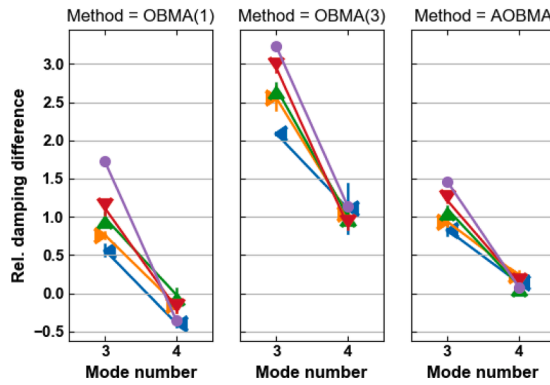


Fig. 28. Relative damping ratio errors of matched mode estimations, 25 Hz analysis bandwidth (for the legend refer to Fig. 26).

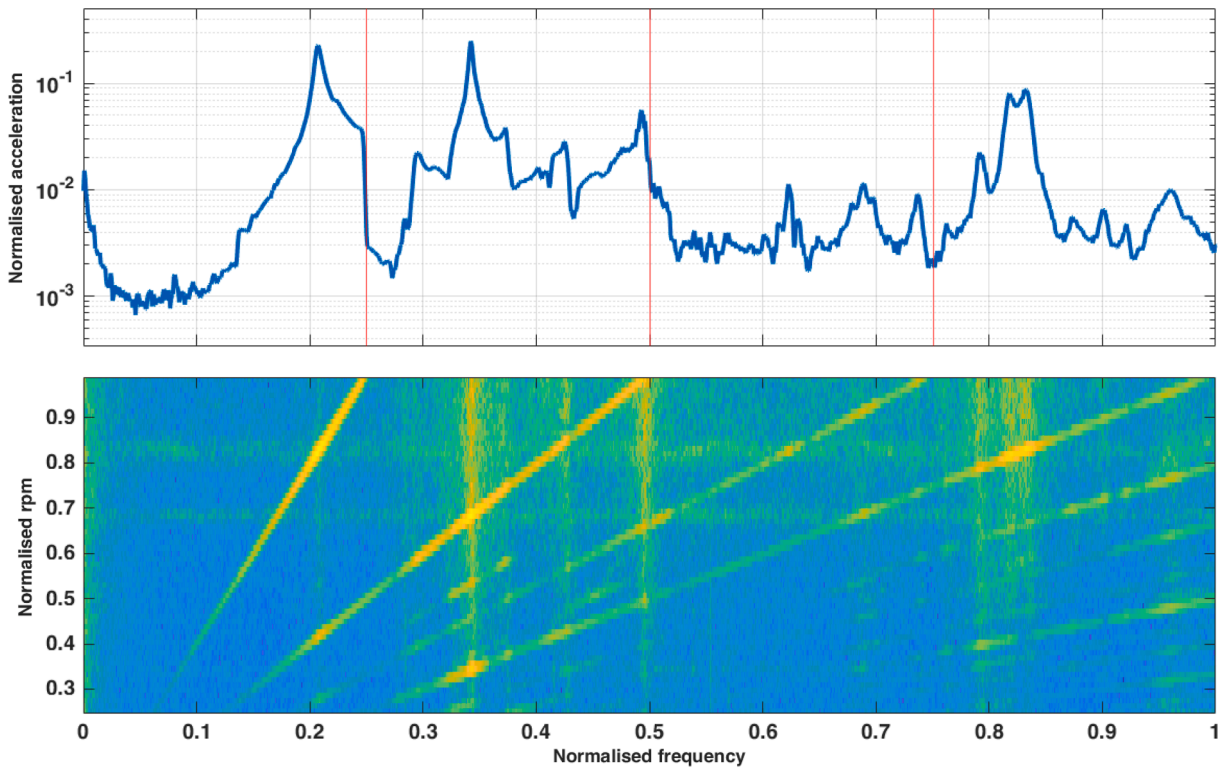


Fig. 29. Acceleration spectrum (top) and spectrogram (bottom) from operational run-up data.

The averaged difference function $\bar{d}_{l,l+1}$ between subsequent orders can then be used to eliminate the magnitude differences, which are due to different input order amplitudes a_l between those orders. This aligns the magnitudes of the output orders to facilitate subsequent order averaging.

To apply the presented method beyond the common (i.e. intersecting) frequency range of all orders, the edge values of the difference functions $\bar{d}_{l,l+1}$ in Eq. (8) are extended to cover the full frequency range of order l . This ensures that the final averaged spectrum covers a frequency range, which is a union (and not just an intersection) of the individual orders' frequency ranges. This is a benefit of AOBMA compared to OBMA, where the spectral content is divided into several orders with different, partially overlapping frequency ranges.

A difference function can be computed between arbitrary orders l and $o > l$ by multiplying the difference functions of intermediate orders:

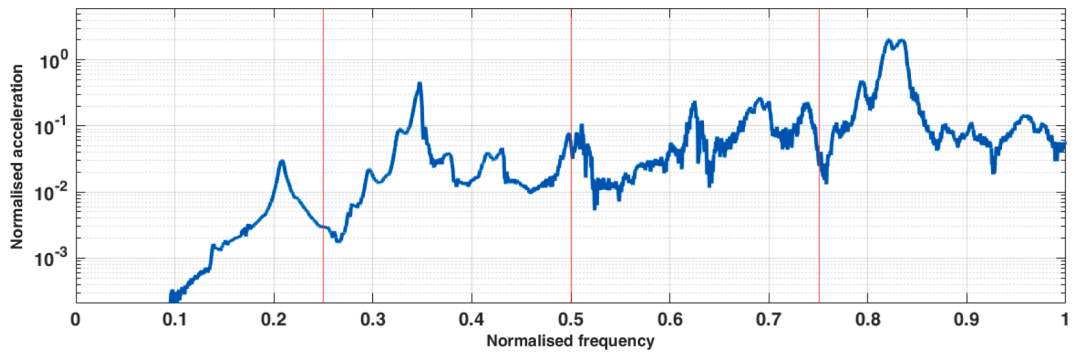


Fig. 30. Acceleration magnitude spectrum from scaled and averaged orders (AOBMA).

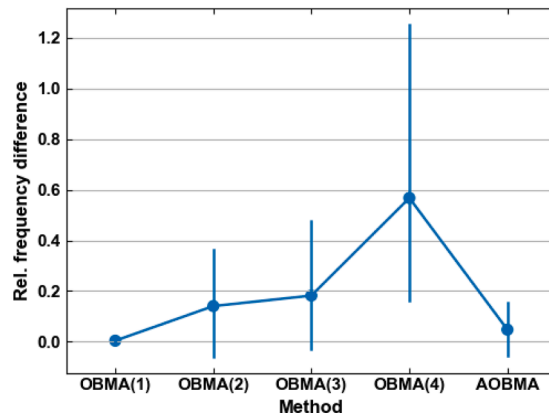


Fig. 31. Mean eigenfrequency differences relative to OMA results.

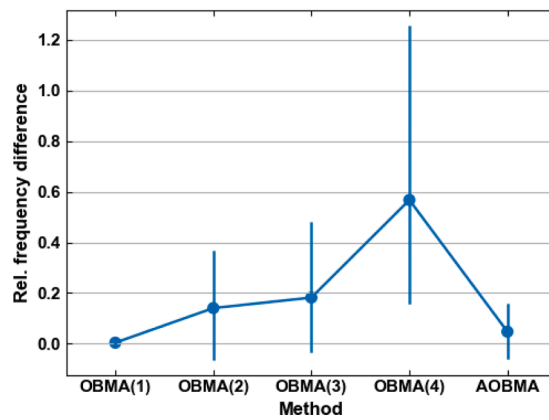


Fig. 32. Mean damping ratio differences relative to OMA results.

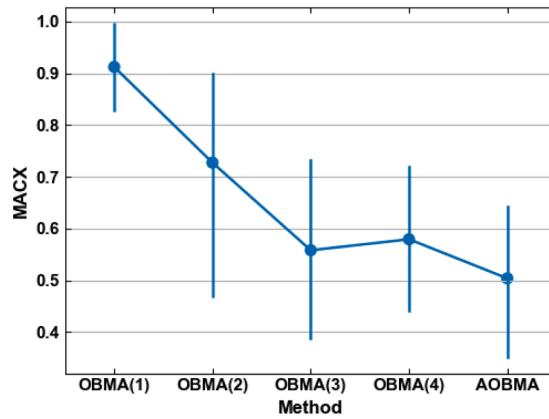


Fig. 33. Mean MACX values between mode shape results from OMA and the specified methods.

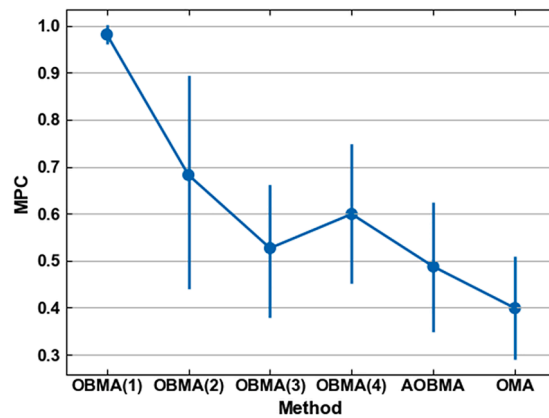


Fig. 34. Mean MPC values of mode shape results from all methods.

$$\bar{d}_{l,o}(f) = \prod_{i=l}^{o-1} \bar{d}_{i,i+1}(f) \tag{9}$$

The highest order o is selected as the reference to calculate scaling factors for the remaining orders according to Eq. (9). At every frequency value f , spectrum values of the order l are divided by the difference ratio values $\bar{d}_{l,l+1}$ as per Equation (10). This results in spectra of order l with magnitudes scaled to the input order amplitude a_o of the reference order o .

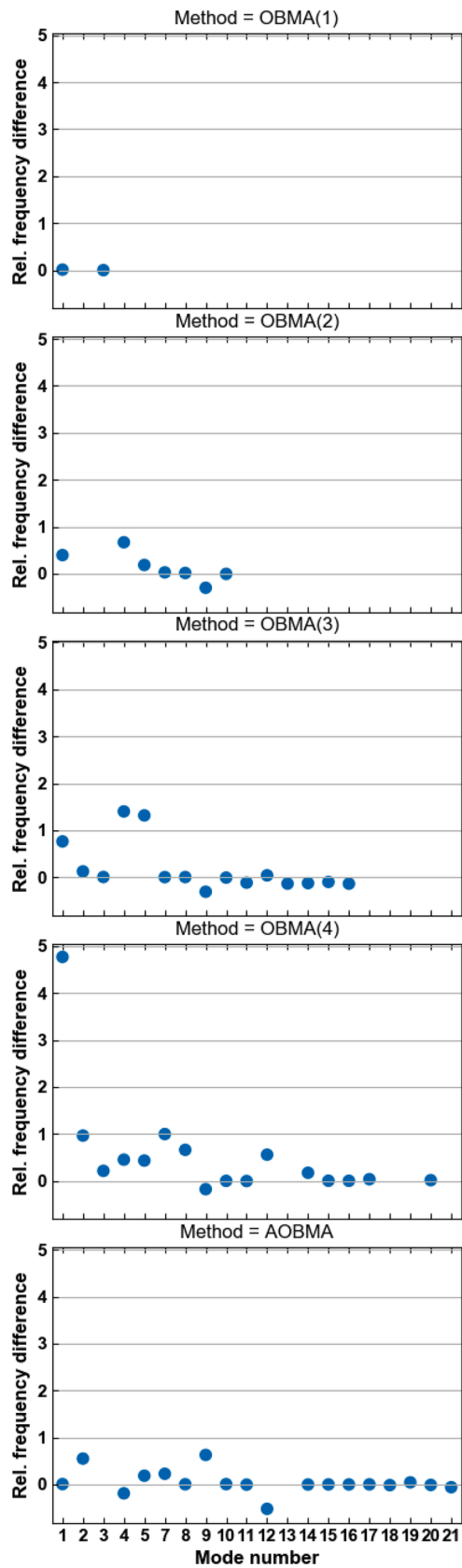
$$\frac{1}{\bar{d}_{l,o}(f)} [S_{yy,l}(f)] = [S_{yy,l}(f)]_{a_l=a_o} \tag{10}$$

Finally, the scaled orders $l..o$ are averaged over common frequencies f :

$$\left[\bar{S}_{yy}(f) \right] = \frac{1}{o-l+1} \sum_{i=l}^o [S_{yy,i}(f)]_{a_i=a_o} \tag{11}$$

For simplicity, Equation (11) shows an average of the orders with equal weighting. Alternatively, a weighted average can be applied to emphasize the influence of the most significant orders. In the present work, a frequency-dependent weighted averaging of orders based on the original (unscaled) order magnitudes was implemented to favour orders with higher energy content at individual frequency values. This addresses the issue that the quality of results from OBMA depends noticeably on the chosen order as observed in [10]. The approach also extends a previous work [7], where significant orders were chosen for OBMA without further consideration of frequency-dependence. This is relevant in the sense that a certain order might be suitable for a certain frequency range, while modal identification in a different frequency area might benefit from a different order.

Because a higher frequency modulation rate increases distortions of obtained order spectra [25,26] (further discussed and



(caption on next page)

Fig. 35. Eigenfrequency differences $(f_{est} - f_{OMA})/f_{OMA}$ relative to OMA results.

illustrated in the following subsection with Fig. 9), it can be reasonable to assign a greater weight to lower orders. This can be done explicitly, e.g. by taking the inverse of the order number as the weighting factor for the corresponding order spectrum. However, the mentioned magnitude-weighting accomplishes that implicitly because order input forces typically increase as a function of rpm while the rate of frequency progression is order-dependent as shown in Equation (1). That is, lower orders have a higher rate of increasing magnitude over their order frequency compared to higher orders.

2.4.1. Implementation and application of AOBMA

While the last section serves as a theoretical description, the paragraphs below focus on aspects of the practical implementation of AOBMA, such as the presence of discretely sampled data. This section also illustrates the methods' application using the same simulated response data, which was presented earlier in Section 2.3 and which is further described in the following Section 3.1.

Since orders are extracted as a function of rpm or time, the first step is to interpolate the orders to common frequency values. Let F_l be such set of discrete frequencies $f_{l,i}$ with samples i of order l after the interpolation. The overlapping frequency range $F_{l \cap l+1}$ of two subsequent output order functions, $y_{l,i}$ and $y_{l+1,b}$ is determined as $F_{l \cap l+1} = (F_l \cap F_{l+1})$.

Next, relative difference functions \bar{d}_{l+1} of the orders' magnitudes are calculated for all $f_{l \cap l+1,i} \in F_{l \cap l+1}$ according to Eq. (7) for each channel individually. A noise reduction can be achieved by averaging the resulting difference functions for each subsequent order across all channels as per Equation (8).

If the lower order l covers frequencies outside the frequencies of the higher order $l + 1$, i.e. if $F_l \setminus F_{l+1} \neq \emptyset$ (where \setminus denotes the relative complement in set theory), values at the edges of \bar{d}_l are extended to cover the full frequency range F_l of order l .

Fig. 6 shows the averaged difference functions \bar{d}_{l+1} between all subsequent orders of a simulation run (using harmonic ratio 0.8, Eq. (12)). The left part of the illustration is based on orders extracted from the acceleration response of the structure. For validation, the right section provides scaling functions, which are determined from input force orders directly. Recall that the goal is to determine (and afterwards to reduce) the magnitude trend difference between response orders due to different amplitudes of input orders. Order difference functions (Fig. 6, left), which were determined from the tracked response orders follow the overall progression of the true difference functions (Fig. 6, right) of the inputs. This underlines that these input force differences in fact can be estimated from the response signal.

However, noticeable deviations occur at resonant frequencies of the structure and are visible as spikes (Fig. 6, left). These spikes are explained by distortions in the response order spectra at resonance peaks [25,26], shown in Fig. 9. They occur when relating the instantaneous sweeping excitation frequency to the response frequency and depend on the sweep rate of the excitation [27]. The averaging of order scaling functions across different channels does not alleviate these distortions as they are present across different channels. However, uncorrelated noise is reduced, which is visible in the output order difference functions (Fig. 6, left), where averaging across all 18 channels is used. In contrast to that, the plots of the input order difference functions (Fig. 6, right) are based on an average of just 2 signals (from order excitations in X and Y direction) and thus show greater noise.

Afterwards, a moving average is applied to the scaling functions \bar{d}_{l+1} . This ensures that 1) the noise in the difference functions is further reduced while preserving the estimated difference trend and 2) the sharp peaks in Fig. 6 (left) due to the mentioned resonance distortions are alleviated. Alternatively, a fitting function can be determined for \bar{d}_{l+1} , e.g. from polynomial fit by employing the least-squares method. The resulting estimated trend function is denoted \tilde{d}_{l+1} .

To find the direct trend relation between each order to the highest present order, the subsequent order difference functions of higher orders are multiplied as explained by Eq. (9). For example, the scaling of order $l = 4$ to order $o = 8$ is determined as $\tilde{d}_{4,8} = \tilde{d}_{4,5} \tilde{d}_{5,6} \tilde{d}_{6,7} \tilde{d}_{7,8}$. Fig. 7 shows the resulting trend difference estimations from each order to the highest tracked order.

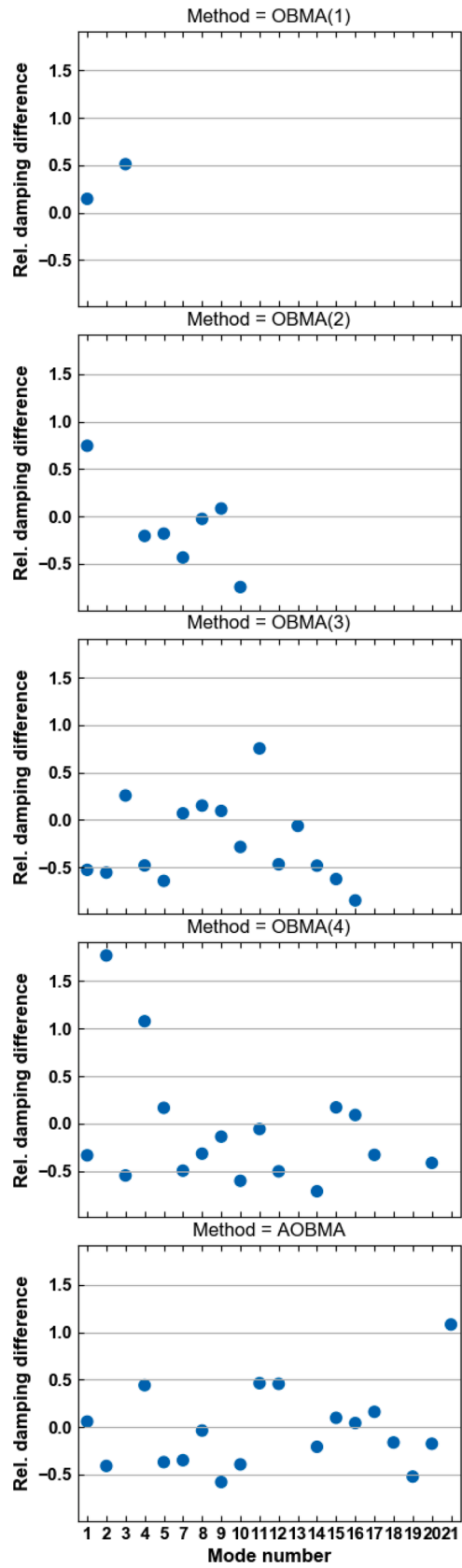
According to Eq. (10), the estimated trend differences $\tilde{d}_{l,o}$ are used to scale the magnitude of each order $|y_l|$ to the common magnitude level of the highest order $|y_o|$. Fig. 8 shows the individual orders in their original (unscaled) and resulting scaled form. It is visible that the magnitudes of the scaled orders (plotted as bold lines) align well to the highest order.

Zooming into the first resonance peak in Fig. 9 shows that small-scale differences between orders are preserved while the magnitude level alignment is ensured along the whole frequency range.

The distortion impact of higher orders on the resonance spectrum is visible in Fig. 9. Detailed discussions on this phenomenon can be found in [25,26]. The effect is especially pronounced on lightly damped modes, which is also the case here. With greater excitation sweep rates (i.e. higher orders), two effects are observed:

1. The resonance peak is shifted to the sweeping direction, which can lead to an overestimation of natural frequencies in case of a positive sweep rate as in the present simulation. Vice versa, a negative sweep rate (i.e. decreasing excitation frequency over time) would promote an underestimation of natural frequencies.
2. The resonance peak becomes flatter, which produces an overestimation of the modal damping.

Finally, the orders can be averaged into the result shown in Fig. 10 using Eq. (11). In contrast to the overall response spectrum in Fig. 2, the resulting average does not show discontinuities at the ending frequencies of orders. In comparison to the individual orders in Fig. 4, the averaged magnitude is aligned to a common level and the phase signal shows less noise. Furthermore, the partial frequency



(caption on next page)

← **Fig. 36.** Damping ratio differences $(\xi_{est} - \xi_{OMA})/\xi_{OMA}$ relative to OMA results.

ranges of individual orders are combined into a single spectrum signal covering their full combined frequency range.

The present study focuses on the dynamic response of a stationary structure, which is subjected to periodic excitation by a contiguous rotating structure, like a fan or disc assembly. It should be noted that this rotating structure itself can exhibit rpm-dependent natural frequencies due to gyroscopic effects [28]. On the stationary structure, these resonances would thus emerge as an excitation with rpm-dependent amplitude and become part of the measured response of the combined system. The order spectra are associated with the individual order frequencies, which differ from the rpm by the factor l , Eq. (1). This means that the measured response peak arising from an rpm-dependent eigenfrequency of the rotating structure would occur at different frequencies for different tracked orders. This has to be considered during the smoothing (e.g. by a suitable moving average window size), so that the sharp distortions shown in Fig. 6 (left) are removed while amplitude changes due to rpm-dependent eigenfrequencies are preserved in the difference functions. Otherwise, there is a risk that a single rpm-dependent mode contributes to the averaged signal with multiple peaks at different frequencies. Besides that, when each order is scaled to the highest order in AOBMA (Eq. (10)), the resulting averaged order spectrum will correspond to this highest reference order in terms of the rpm-dependent eigenfrequencies. While the present study does not further consider the influence of rpm-dependent eigenfrequencies, such conditions can be assessed further in the future with a data set, which incorporates gyroscopic effects.

3. Methodology

Acceleration responses from a parametric simulation study as well as operational measurements of a turbofan casing during acceleration are used in this study. The purpose is to validate the novel AOBMA method and to compare the modal estimation performance of OMA, OBMA and AOBMA. Both datasets are introduced in the following subsections together with the used analysis methodology.

3.1. Parametric simulation study of a 2D spring-mass-damper system

The simulated 2D structure consists of 9 nodes, which represent point masses and are connected with spring and dashpot elements with a total of 18 degrees of freedom. The parameters of the structure's elements and its geometry are provided by Table 1 and Fig. 11, respectively.

External forces are applied at the central node 9 in both the X and Y direction. These forces consist of combined random input and a rotating force vector in the XY-plane to simulate unbalance and harmonics, which produce individual orders l . In the parametric study, the harmonic ratio is introduced as an independent variable, which adopts the set of values given in Eq. (12). It describes the ratio of harmonic (i.e. order) RMS amplitude $\text{RMS}(x_l(t))$ to the sum of harmonic and random RMS amplitudes $\text{RMS}(x_l(t)) + \text{RMS}(x_r(t))$:

$$\frac{\text{RMS}(x_l(t))}{\text{RMS}(x_l(t)) + \text{RMS}(x_r(t))} \in \{0.2, 0.4, 0.6, 0.8, 1.0\} \quad (12)$$

The total duration of each simulation run is $T = 100$ s. While the harmonic ratio is kept constant per simulation run, the sum $\text{RMS}(x_l(t)) + \text{RMS}(x_r(t))$ is linearly increased over time t according to Eq. (13), where $\Sigma_{t1} = 200$ N and $\Sigma_{t2} = 4000$ N are the RMS sums at the beginning and end of a simulation run, respectively.

$$\text{RMS}(x_l(t)) + \text{RMS}(x_r(t)) = \Sigma_{t1} + (\Sigma_{t2} - \Sigma_{t1}) \frac{t}{T} = 200\text{N} + 3800\text{N} \frac{t}{T} \quad (13)$$

The frequency f_1 of the first order $l = 1$ (i.e. the fundamental frequency) is increased linearly from $f_{1,t1} = 5$ Hz to $f_{1,t2} = 30$ Hz over time as specified by Eq. (14). This equates to a run-up from 300 rpm to 1800 rpm.

$$f_1(t) = f_{1,t1} + (f_{1,t2} - f_{1,t1}) \frac{t}{T} = 5\text{Hz} + 25\text{Hz} \frac{t}{T} \quad (14)$$

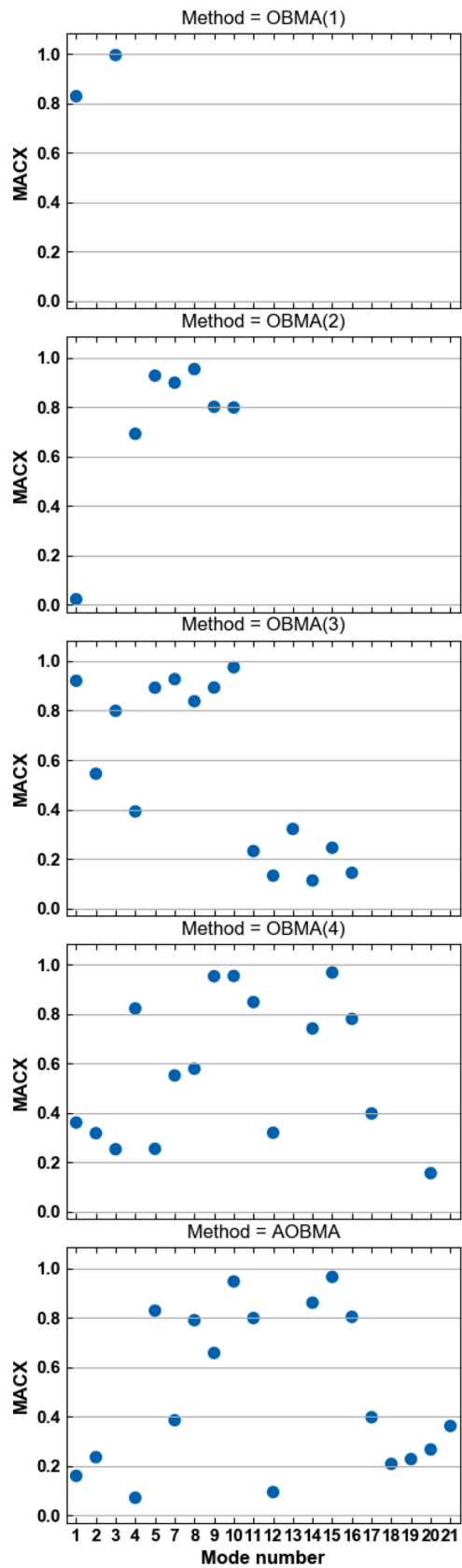
The first 8 orders are included in the excitation with frequencies defined by Eq. (15).

$$f_l(t) = l f_1(t), l \in \{1, 2, 3, 4, 5, 6, 7, 8\} \quad (15)$$

Each distinct harmonic ratio below 1.0 is simulated with 30 runs each to determine the means and confidence intervals of estimated modal parameters. The harmonic ratio of 1.0 is simulated by a single run due to the deterministic nature of the purely harmonic order excitation. Therefore, the resulting Monte Carlo parametric simulation study features a total of 121 simulation runs.

The reference modal parameters of the presented structure are determined from a complex eigenvalue analysis of its system matrices. The undamped eigenfrequencies and damping ratios are presented in Table 2. Even though not immediately obvious from the geometry (Fig. 11), the structure has two rigid body modes. These are listed as modes 1 and 2 with zero damping in Table 2.

All compared modal estimation methods (OMA, OBMA and AOBMA) were first applied to a small subset of randomly selected simulation runs to determine a suitable range of common stabilisation criteria for modal identification. Within the determined range of stabilisation criteria, 4 different combinations of frequency and damping tolerances were then used in a batch analysis of all simulation runs to estimate the potential impact of the stabilisation criteria on the obtained results. The modal parameter results from the 3



(caption on next page)

← Fig. 37. MACX values between mode shape results from OMA and the specified methods.

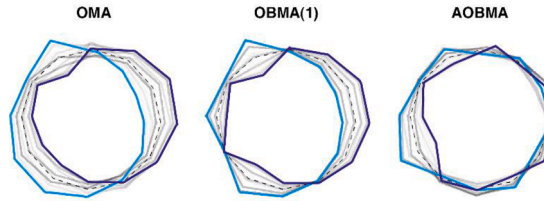


Fig. 38. Overlaid deflections of mode 1 estimated by OMA, OBMA(1), AOBMA.

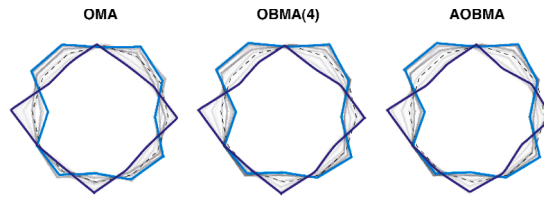


Fig. 39. Overlaid deflections of mode 15 estimated by OMA, OBMA(4), AOBMA.

estimation methods were then stored for a subsequent comparison with the reference results (i.e. eigenfrequencies, damping ratios and mode shapes) from the simulation. The main trends and observations remained consistent within the range of tested stabilisation criteria. A final representative set of stabilisation criteria is used for the presented results and is given in Table 3.

The Pole-weighted Extended Modal Assurance Criterion (MACXP) [13] is utilised to match estimated modes to reference modes. First, a matrix of MACXP values is constructed between the numerical reference modal parameters and the modal estimation set from a simulation run. This step is analogous to the construction of the more common MAC matrix. In contrast to the MAC value, however, the MACXP is less sensitive to mode shape complexity and also considers natural frequencies and damping ratios of the compared modes (see Section 2.2 for more details). Higher values of the resulting MACXP matrix indicate matching modes, which are then compared further. Additionally, tolerances of the relative estimation errors are introduced as matching criteria. In the present case, the estimated eigenfrequency f_{est} (quantified by the relative error) and mode shape (quantified by the MACX) of the estimation must stay within the tolerances specified by Table 4 to be considered a matched mode. These values were chosen to exclude outliers from the comparison and declutter the comparison plots. Estimations, that do not meet these tolerances are defined as unmatched modes and can occur due to noise, end-of-order modes, or numerical spurious modes.

Estimation results from the individual methods, OBMA, AOBMA and OMA are compared later in Section 4.1.

3.2. Operational run-up of a turbofan casing

To validate the presented AOBMA method in a real-world test case, it is also applied to operational vibration data of a mechanical spinning test. The estimation results are then compared to outputs from OMA and OBMA.

The used mechanical test rig hosts a fan/casing assembly of a commercial turbofan engine. The fan is driven directly by an electromagnetic motor. Due to the lack of combustion and environmental forces, an increased contribution of harmonic order input is expected in relation to random excitation amplitudes. The fan casing is instrumented with accelerometers at 12 positions illustrated in Fig. 12. One triaxial accelerometer is used at position 4. The remaining positions host 11 uniaxial accelerometers oriented in the normal direction of the cylindrical surface area of the casing. Hence, a total of 14 accelerometer data channels is recorded. In addition, the rotation speed is acquired from a pulse signal reading. The measurement signals are sampled at a frequency of 65 kHz but low-pass filtered and downsampled to achieve a lower Nyquist frequency of interest. Such a high sampling frequency is used as standard practice in the test facility, which conducted the measurement campaign to provide leeway in the acquired bandwidth against potential contingencies during the test. The analysed measurement data covers a run-up of the fan with the lowest acceleration rate provided by the fan speed control unit, resulting in a measurement duration of 190 s.

In contrast to the simulation-based analysis from the previous section, true reference modal parameters of the real tested structure are unknown. Therefore, modal estimation results from traditional OMA are used as the baseline to compare and validate results from OBMA and AOBMA. The same procedure as described in the previous section is used to find matching modes for the comparison of their estimated parameters by different methods.

4. Results and discussion

The first subsection below uses data of the parametric simulation study (Section 3.1) to compare the estimation accuracy of OMA, OBMA and AOBMA while considering the potential impact of the harmonic ratio. Afterwards, the three methods are applied to operational measurements of the test setup presented in Section 3.2.

4.1. Comparative performance assessment of OMA, OBMA and AOBMA

In the following, OMA, OBMA and AOBMA are first applied to the maximum frequency range available to each method in Section 4.1.1. In the subsequent Section 4.1.2, the results of an additional approach based on averaging of OBMA results in post-processing are introduced and discussed. Finally, OBMA and AOBMA are applied to a common, narrowed analysis bandwidth (covering modes 3–4 only) to isolate the impact of the analysis band on the estimation performance.

Only orders $l \in \{1, 3, 5, 8\}$ of the simulation are used for the following OBMA results and the specific source order is specified in brackets as OBMA(l). This reduced set of orders is used to support conciseness of the following plots and discussions. The included orders are selected to be spread approximately equal across the range of all orders. All 8 excitation orders are simulated with the same amplitude function over rpm or time (Eq. (13)), so there is no inherent preference of the picked orders of the subset and their individual differences are limited to the sweep rates and covered frequency ranges. The same reduced set of 4 orders is also processed within the presented AOBMA results below to ensure better comparability.

4.1.1. Modal estimations over the maximum frequency range of each method

In this section, the maximum frequency range of each method is used for modal analysis. For OMA, an analysis band from 0 Hz to 270 Hz is chosen to cover all eigenfrequencies (Table 2). The full frequency bands of individual orders, determined by Eqs. (14) and (15), are used for OBMA. Consequently, their combined frequency ranges provide the used analysis band of 5 Hz to 240 Hz for AOBMA.

Fig. 13 shows for each mode (on the horizontal axis) the count of simulation runs (on the vertical axis), where this mode was matched according to the criteria from Table 4. Since there are 30 simulation runs per discrete harmonic ratio below 1.0, the maximum number of matches per mode and harmonic ratio is 30. An exception is the purely harmonic (and thus deterministic) excitation with a harmonic ratio of 1.0, where only 1 simulation run was performed. Focusing on OBMA(l), it is evident that the range of matched reference modes on the horizontal axis increases if a higher order l is used. This is simply due to the increasing frequency range, which is covered by higher orders.

Within individual methods, the overlaid plots of harmonic ratios are mostly consistent, except for certain modes that are more challenging to identify. This is the case for reference modes number 3 and 4, which have close natural frequencies with a difference below 0.5 Hz (Table 2). OBMA(1) and OMA achieve the highest number of matches for these modes. The difference between the results of OBMA(1) and OBMA(3) is likely due to the increased distortion of the spectrum of order 3 compared to order 1 (Fig. 9). OBMA(1) results in a substantially higher number of matched estimations of mode 3 compared to AOBMA. Whether this is due to the smaller frequency range of OBMA(1) or a potential impact of order averaging by AOBMA will be evaluated in Section 4.1.3.

Another clear dip in the number of matches appears in OBMA(8) at mode number 10 and is also reflected in AOBMA. However, this dip is limited to a low harmonic ratio of 0.2. OMA identifies this mode only once in the 121 simulation runs. Between modes 5–12, the proposed AOBMA method is free of gaps in contrast to OMA and shows a less pronounced dip compared to OBMA, which can be attributed to a noise reduction by averaging of orders. Modes 13 and up are not identified by OMA either. A reason might be the increased damping ratios of these modes in combination with the end-of-order effect, which produces small-scale distortions of the spectrum as shown in Fig. 2. AOBMA and OBMA(8) are able to identify these higher modes, albeit with a trend that higher harmonic ratios lead to a greater number of matches.

None of the methods successfully matched mode 18. The reason is that the maximum frequency of the highest order 8 (240 Hz) is very close to this mode's eigenfrequency (239.84 Hz). This mode is therefore not sufficiently covered by the frequency range of OBMA (8) and AOBMA. While this restriction does not apply to OMA, it is not able to identify this mode either, likely due to the substantial end-of-order distortion of the spectrum at this frequency, which is visible in Fig. 2.

The results can be summarised with Fig. 14 (left), which shows how many different modes from a single simulation run have been matched on average. Each data point represents the mean value of 30 simulation runs (for harmonic ratios below 1.0). The vertical error bars extending from the data points visualise 95% confidence intervals around the mean.

It is visible that OBMA(8) and AOBMA benefit from higher harmonic ratios while OMA is mostly unaffected. However, even at low harmonic ratios of 0.2 and 0.4, the number of modes matched with AOBMA approaches the number of modes matched with OMA. Overall, the proposed AOBMA method provides the greatest number of matched modes.

For completeness, Fig. 14 (right) also shows the count of unmatched modes, which exceed the tolerances from Table 4. Only a minor impact of the harmonic ratio is visible: the low harmonic ratio of 0.2 results in slightly elevated unmatched count values, especially in OBMA(8) and AOBMA. Unmatched count values of the harmonic ratio 1.0 follow the overall trend more coarsely because each plotted point is based on a single sample (i.e. simulation run). In contrast to that, data points of other harmonic ratios are based on 30 samples, resulting in more representative average values. OBMA(1) shows the highest amount of unmatched modes compared to OBMA results of higher orders because order 1 covers the smallest frequency range and the modal model is overfitting resulting in spurious mode estimations. The dip of the number of unmatched modes in OBMA(8) is also explained by the frequency range of order 8, which starts at 40 Hz and thus omits the challenging modes 3–4, as seen in Fig. 13. Finally, AOBMA and OMA show similar counts of unmatched modes in Fig. 14 (right) despite more matched modes in favour of AOBMA in Fig. 14 (left).

Next, the accuracy of the methods regarding individual estimated modal parameters of the matched modes is compared.

Fig. 15 shows the relative errors of estimated eigenfrequencies. Considering the error tolerance of $\pm 1\%$ (Table 4) and the consistency of the results in Fig. 15 (with limited outliers), the accuracy of estimated eigenfrequencies in this simulation study is high across all methods. An impact of the harmonic ratio is visible in the form of more accurate estimations with increasing harmonic ratios in order-based methods. For example, this is the case for the mode 4 of OBMA(3), modes 14–16 of OBMA(8) and AOBMA. A stronger impact of harmonic ratios was observed and discussed in the previous results of Fig. 13 and Fig. 14. In contrast to that, the overall impact on the estimation accuracy of modal parameters is minor since the graphs of different harmonic ratios mostly overlap for all modal estimation methods.

Therefore, hereafter, results of individual harmonic ratios are averaged into single plots to increase conciseness and facilitate the comparison of the methods by overlaying their plots. Fig. 16 combines the eigenfrequency results from Fig. 15 in such way.

In Fig. 16, the result of averaging with the proposed AOBMA method is visible. Aside from mode 3, which is also based on much fewer AOBMA estimation samples (Fig. 13), AOBMA produces more consistent results compared to OBMA and mitigates increased error values of OBMA(8) at modes 6–7. Eigenfrequencies of lower, lightly damped modes are overestimated by the order-based methods OBMA and AOBMA due to the distortion effect described with Fig. 9.

The same effect is also responsible for the large overestimation of damping ratios (with differences up to approximately 200%) by OBMA, which are shown in Fig. 17. It is visible that higher orders produce greater overestimations compared to lower orders used within OBMA, which is in conjunction with earlier observations from Fig. 9. AOBMA reduces these error deflections and delivers more consistent results compared to individual OBMA outputs because the negative impact of higher orders is mitigated by spectrum averaging with lower orders carrying less distortions. This is additionally reinforced by a weighted averaging in AOBMA, which implicitly favours the contribution of lower orders as noted in the ending paragraphs of Section 2.4. As a result, the accuracy of eigenfrequency and damping ratio estimations by AOBMA approaches the results from OMA, which is not affected by the order spectrum distortion effect.

In Fig. 18, the estimation performance of mode shapes is quantified by MACX values, which are calculated between the matched mode estimations and the true reference mode shapes of the simulated structure. The graph shows that OBMA and AOBMA provide similar results and clearly surpass OMA in the estimation of mode shapes: while the difference is small in modes 5–7, greater differences are visible in modes 8–12, where OBMA and AOBMA still provide MACX values close to 1. A decreased mean and increased variance of MACX values from OBMA and AOBMA is visible at mode 14 and up. The discrepancy between the performance of OBMA/AOBMA and OMA is likely related to the present excitation condition (mixed random and correlated harmonic order excitation at a single location).

For a closer analysis, Fig. 20 is limited to modes 6–12 and shows the degree of mode shape complexity using the MPC value for individual levels of the harmonic ratio. In addition, 30 simulation runs with a harmonic ratio of 0.0 (i.e. purely random excitation) are included in the analysis by OMA. The mode shape estimation of OMA seems to be affected by the phase of the (sweeping) order input, resulting in increased complexity of the estimated mode shapes. OBMA and AOBMA, on the other hand, provide consistently low mode shape complexity (with MPC values close to 1) for harmonic ratios of 0.2 and up.

This is also supported by an observation of the estimated mode shapes on the structure. For example, Fig. 19 shows the overlaid deflections of a vibration cycle for the mode shape estimation of mode 12 at harmonic ratio 0.8 by OMA (left) and AOBMA (right). At the illustrated scale, the AOBMA mode shape is indistinguishable from the reference mode shape and shows antisymmetric deflections. The OMA estimation (Fig. 19, left), on the other hand, matches these reference deflections well on the right part of the structure (e.g. at node 6, Fig. 11) but fails to do so at the nodes of the left half of the structure. In addition, the impact of the rotating excitation on the OMA estimation is visible, resulting in a circular motion of the central node illustrated by the ellipsoidal trace line in Fig. 19 (left). This in turn explains a decreased MPC value of the OMA estimation (Fig. 20). During order tracking, each tracked response order is phase-referenced with a sinusoidal reference signal of the input order, which is synthesised using the rpm signal and the corresponding order number [19,29]. It appears that OBMA and AOBMA benefit from this phase-referencing of the output signal, leading to a more accurate mode shape estimation.

4.1.2. Averaging of OBMA results in post-processing

This section presents and discusses results obtained from an alternative averaging approach. Instead of averaging of order spectra in pre-processing as presented before, the modal estimations of each mode obtained from OBMA are averaged across different orders in post-processing. In the following, this method is denoted “Post-AOBMA” and averages the previously presented results of OBMA estimations from orders 1, 3, 5, 8. In analogy with the weighted averaging in AOBMA (Section 2.4), a higher weighting of lower orders is also implemented in Post-AOBMA by using the inverse of the order number as the weighting factor for modal estimations from the corresponding orders. The following plots in Fig. 21 to Fig. 24 show the modal estimation performance of Post-AOBMA. For reference, the previously presented results of AOBMA and OBMA(8) are included as well.

In Fig. 21, Post-AOBMA shows a higher number of simulation runs with matched modes compared to AOBMA results for modes 3–4 and for a harmonic ratio of 0.2 in the range of modes 8–10. The reason is that Post-AOBMA benefits from the fact that OBMA(1) and OBMA(3) more often identify modes 3–4 while OBMA(5) more often identifies modes 8–10 compared to AOBMA (Fig. 13). However, this elevated performance of OBMA(1) and OBMA(3) is also due to their smaller frequency band and comes at the cost of increased spurious modes as discussed with Fig. 14 (right). This question is further evaluated in the following Section 4.1.3. Moreover, in the presented setup, Post-AOBMA has the advantage that averaged OBMA results of individual orders are already matched to a set of true reference modal parameters. In a real-world application of Post-AOBMA (where true modal parameters are unknown) the mode matching should be performed between individual OBMA results themselves. While this can be implemented algorithmically (e.g.

utilising the MACXP), it constitutes an error source for Post-AOBMA results, which is not considered here. In contrast to that, this requirement of mode matching between orders does not apply to AOBMA because it is based on pre-processing.

From Figs. 22–24 it is visible that, in the upper frequency range, the results of Post-AOBMA are identical to those of OBMA(8), which is due to the lack of other orders' contributions in the frequency range of mode 12 and up (Fig. 13). For the closely spaced modes 3–4, Post-AOBMA shows favourable performance in the estimation of modal parameters. However, this performance is likely elevated due to factors discussed in the previous paragraph. Leaving aside modes 3–4, AOBMA shows a greater mean estimation performance for all modal parameters compared to Post-AOBMA. This is also the case for mode numbers above 11, even though both AOBMA and Post-AOBMA are solely based on order 8 in this frequency range since order 5 ends at 150 Hz. However, this can be related to a reduced number of modes identified in this frequency range (Fig. 13), contributing to a higher uncertainty of the results indicated by larger vertical bars, especially visible in Fig. 24. Besides that, averaging by AOBMA reduces the variance in the processed spectra, potentially leading to a reduced error bias during the modal estimation. It was shown that averaging of the frequency spectrum has an impact on modal estimation performance, albeit primarily on the variance of modal parameters estimated in (regular) OMA by the pLSCF method [30].

4.1.3. Comparison of OBMA and AOBMA at a common, narrowed analysis bandwidth

Due to different frequency ranges of individual orders (Eq. (15)), the previously presented results are obtained not only by different estimation methods but also utilise different analysis bandwidths. Great estimation differences of modes 3–4 between OBMA(1), OBMA(3) (and consequently Post-AOBMA) on one hand and AOBMA on the other hand were observed in Sections 4.1.1 and 4.1.2. Therefore, this section compares the estimation performance of these methods using the common analysis bandwidth of 25 Hz covering modes 3–4. More precisely, the analysis band of AOBMA is reduced to match the frequency range of OBMA(1), i.e. 5 Hz–30 Hz. The analysis band of OBMA(3) is shortened to cover the same bandwidth of 25 Hz, resulting in a range of 15 Hz–40 Hz. This alleviates the advantage of Post-OBMA noted in Section 4.1.2 for a clearer comparison and allows to gauge a potential impact of order averaging on the estimation of closely spaced modes. The same stabilisation criteria are used for the following results as before (Table 3), except for the required minimum number of stable poles, which is increased to 10 to avoid overfitting with identifications of spurious modes.

As expected from previous discussions (Fig. 9), OBMA(3) mostly shows a decreased performance compared to OBMA(1) in Fig. 25 to Fig. 28 because of the increased spectrum distortion at higher frequency modulation rates of higher orders. In AOBMA, the spread of modal parameter estimations between different harmonic ratios (Fig. 25 to Fig. 28) appears smaller compared to OBMA(1) and OBMA(3). This indicates a positive effect of AOBMA at low harmonic ratios, which show a decreased performance in OBMA(1) and OBMA(3), especially at the eigenfrequency (Fig. 27) and damping ratio (Fig. 28) estimations. Overall, AOBMA does not show worse results compared to OBMA(3) and partially surpasses the performance of OBMA(1). Based on this, it can be concluded that the estimation of the closely spaced modes 3–4 is not negatively affected by order averaging in AOBMA compared to OBMA. Instead, the estimation performance benefits from a narrow analysis band in this range.

4.2. Operational run-up of a turbofan casing

In this section, first, spectra from the unprocessed time response are compared to the response spectrum estimate from the proposed AOBMA method. Afterwards, differences in modal parameter estimations between OBMA and AOBMA in relation to OMA are presented and discussed.

In the following, rpm, frequency (f_{norm}), and amplitude values are provided in normalised units, which are scaled in relation to their respective maximum values in the analysed measurement.

Fig. 29 shows a spectrum from the response in radial direction at position 4 (Fig. 12). Ending frequencies of orders 1, 2, 3 are highlighted in the graph with red vertical lines. On closer inspection, discontinuities are observed at some of these frequencies. These discontinuities can be attributed to the end-of-order effect. The distortion is especially pronounced at the ending frequency of order 1 ($f_{norm} = 0.25$) and potentially order 2 ($f_{norm} = 0.5$). This stronger impact of the end-of-order effect on frequencies of low orders is in agreement with the observations and explanations from the simulated structure (Fig. 3) in Section 2.3.

The orders 1, 2, 3 and 4 were tracked from the response data and, according to the presented AOBMA method, scaled and averaged, resulting in the spectrum of the same channel shown in Fig. 30. A clear difference in both spectra is visible in the frequency range of the first order. Its impact on the spectrum amplitude is reduced and the discontinuity at its ending frequency ($f_{norm} = 0.25$) is eliminated in Fig. 30. The impact of the second order's ending frequency at $f_{norm} = 0.5$ is difficult to judge from Fig. 29 alone, because it appears to coincide with a resonance. However, the peak at this frequency is reduced in the order-based spectrum in Fig. 30, indicating that an impact of the end-of-order effect on this area is indeed present in Fig. 29.

OMA estimated the most modes with a count of 21, followed by AOBMA with 18 modes. In OBMA, the orders 4, 3, 2 and 1 determined 16, 15, 7 and 2 modes, respectively. In contrast to the simulation data, no tolerance criteria for mode matching are used here, so all modes estimated by OBMA and AOBMA are matched and are included in the following graphs. Another difference to the simulation study is that OMA estimation results are used as reference values since the true modal parameters of the structure are unknown.

Figs. 35–37 show all relative difference values of estimated modal parameters in relation to OMA results for individual modes. The results of individual modes are summarised in Fig. 31–33 into error plots with mean values and confidence intervals of the estimation differences over all modes combined.

Fig. 37 shows that the estimated mode shape of mode 1 has a much greater correlation between OMA and OBMA(1) compared to

AOBMA. These mode shape estimations are plotted in Fig. 38 and clear differences between the estimation methods are visible although they all indicate an overall ellipsoidal deflection, typical for the first circumferential mode of a cylindrical structure. The OBMA(1) mode shape shows symmetry about the horizontal axis but a lack thereof about the vertical axis, while the OMA mode shape seems to be superposed with rigid body motion with clear displacement components along the horizontal axis. In contrast to that, the MACX value indicates consistent results for the mode shape of mode 15 between OMA, OBMA(4) and AOBMA in Fig. 37, which is also confirmed by the mode shapes in Fig. 39.

In Fig. 31, OBMA(1) shows the smallest mean difference and confidence interval in relative eigenfrequency differences compared to OMA. However, this is also promoted by the small frequency range of order 1, resulting in only two estimated modes as shown in Fig. 35. Apart from that, AOBMA delivers estimated eigenfrequencies and damping ratios, which show smaller variance and mean difference compared to OBMA as seen in Fig. 31 and Fig. 32, respectively.

In Fig. 33, the lowest average MACX value is obtained from AOBMA. On first sight, this contradicts the observations from the simulation study in Fig. 18, where MACX values from AOBMA are among the highest. However, here the reference mode shapes originate from (imperfect) OMA estimations while the simulation study uses numerical reference parameters from the eigensolution. As observed in the simulation study, mode shape estimations by OMA were less accurate compared to OBMA and AOBMA. Therefore, low MACX values between OBMA/AOBMA and OMA may indicate less accurate estimations by OMA and not the other way around. This assumption is also supported by the comparison of the mode shape complexity in Fig. 34, where OMA shows mode shape estimations with higher complexity compared to OBMA and AOBMA, which is in conjunction with observations from the simulation study.

5. Conclusions and future work

This work introduced the AOBMA method, which extends OBMA by including intermediate steps of scaling and (weighted) averaging of tracked orders. To validate the proposed method, AOBMA was applied to simulation and real operational data along with OBMA and traditional OMA. Based on this, a comparative study of the three methods was performed to assess their modal estimation performance. In the simulation study, the harmonic ratio was introduced as an independent variable to estimate the impact of harmonic and random contributions in the excitation. The results showed that, with harmonic ratios of 0.6 and up, AOBMA identified a similar or higher number of modes in the specified error range (Fig. 14). However, OMA surpassed the order-based methods in the identification of two very closely spaced modes.

End-of-order distortions are present but relatively limited in the presented simulation, even at high harmonic ratios, as shown in Fig. 2. This likely explains why no clear impact of these distortions and of different harmonic ratios on OMA was observed (Fig. 14, left). However, the spectrum from operational measurements in this paper (Fig. 29, top) as well as previous studies [7–9] illustrate that stronger end-of-order distortions can occur. Since order-based methods are not affected by these distortions, OBMA and AOBMA benefit in such cases, even though it was not observed in the specific simulation study of this paper.

A benefit of the proposed AOBMA method is the reduction of analysis effort in comparison to OBMA, since estimates from individual orders with fractional, partially overlapping frequency ranges are combined into a single data source in AOBMA. The issue of high variance of OBMA results depending on the used order is addressed by AOBMA, as it achieves a noise reduction through averaging of orders and is able to emphasise most significant orders by the application of weighted averaging. As a result, AOBMA provided more consistently low error values of eigenfrequencies and damping ratios compared to individual OBMA results and approached the performance of OMA. This was observed in the analysis results of simulation (Fig. 16, Fig. 17) as well as real operational data (Fig. 31, Fig. 32). The alternative Post-AOBMA method (i.e. averaging of OBMA estimations in post-processing) was examined but does not outperform AOBMA in this study assuming that similar frequency analysis bandwidths are used (Sections 4.1.2 and 4.1.3). Post-AOBMA requires the additional step of mode matching across different orders but is free of the required order scaling and averaging steps of AOBMA. As Post-AOBMA showed an improvement over OBMA results, further research on this method, including algorithmic mode-matching and additional case studies, is suggested.

Regarding mode shape estimation performance, OBMA and AOBMA surpassed OMA in the simulation study (Fig. 18). This observation was also supported by the analysis of real measurements (Fig. 34), even though they lead to a less conclusive assessment due to a lack of true reference mode shapes from the real structure. Order excitation was identified as the likely origin for degraded mode shape estimations in OMA (Fig. 20). In contrast to that, order tracking in OBMA and AOBMA seems to prevent a negative impact of the excitation orders by phase-referencing. To the best of the authors' knowledge, this paper is the first to make this finding, thereby extending the existing use cases for OBMA and AOBMA.

While AOBMA reduces the variance of individual OBMA results, the specific orders used in AOBMA still have a major impact on the achieved results, since the orders form the data foundation of the method. In future work, additional metrics (apart from relative order amplitudes) for the selection of relevant orders and weighting factors for weighted averaging in AOBMA should be evaluated. A correlation-based tool such as the Frequency Response Assurance Criterion (FRAC) could serve to identify and group orders with similar spectra or to create weighting factors depending on the spectrum similarity. This approach can be also useful to determine orders, which meet the assumption of similar force distributions (Section 2.4) and are thus especially suitable for averaging. Moreover, a modal model, which incorporates the distorted shape of resonances in order spectra (Fig. 9) could further enhance the performance of OBMA and AOBMA, especially in the estimation of closely spaced and weakly damped modes. As explained in the ending paragraph of Section 2.4.1, the research on AOBMA can be developed by evaluating the impact of gyroscopic effects in more detail based on corresponding data. Finally, additional independent variables, such as measurement noise or machine acceleration rate, can be included in the simulation study to estimate their impact on the compared methods in the future.

CRediT authorship contribution statement

German Sternharz: Conceptualization, Methodology, Software, Formal analysis, Data curation, Writing – original draft, Visualization. **Tatiana Kalganova:** Supervision, Writing – review & editing. **Cristinel Mares:** Writing – review & editing. **Moritz Meyer-ingh:** Investigation, Resources.

Declaration of competing interest

The authors declare the following financial interests/personal relationships which may be considered as potential competing interests: German Sternharz reports financial support was provided by *EXOLAUNCH GmbH*. Moritz Meyer-ingh reports equipment was provided by *Rolls-Royce Deutschland Ltd & Co KG*. Moritz Meyer-ingh reports a relationship with *Rolls-Royce Deutschland Ltd & Co KG* that includes employment.

Acknowledgements

We would like to express our acknowledgement to *Rolls-Royce Deutschland Ltd & Co KG* for the provision of operational measurement data used in this work.

Funding

This work was supported by *EXOLAUNCH GmbH* and the *Engineering and Physical Sciences Research Council (EPSRC)*.

References

- [1] M. Batel, Operational Modal Analysis - Another Way of Doing Modal Testing, *Sound Vib.* 36 (2002) 22–27. <http://sandv.com/downloads/0208batl.pdf>.
- [2] N.-J. Jacobsen, Separating Structural Modes and Harmonic Components in Operational Modal Analysis, in: *Proceedings of the International Modal Analysis Conference (IMAC)*, 2006, pp. 2335–2342.
- [3] W. Weijtjens, R. Shirzadeh, G. De Sitter, C. Devriendt, Classifying resonant frequencies and damping values of an offshore wind turbine on a monopile foundation for different operational conditions, *IET Renew. Power Gener.* 8 (2014) 433–441, <https://doi.org/10.1049/iet-rpg.2013.0229>.
- [4] P. Mohanty, D.J. Rixen, Operational modal analysis in the presence of harmonic excitation, *J. Sound Vib.* 270 (2004) 93–109, [https://doi.org/10.1016/S0022-460X\(03\)00485-1](https://doi.org/10.1016/S0022-460X(03)00485-1).
- [5] G. Sternharz, T. Kalganova, Current Methods for Operational Modal Analysis of Rotating Machinery and Prospects of Machine Learning, in: *Proceedings of the 38th IMAC: Rotating Machinery, Optical Methods & Scanning LDV Methods*, 2020, pp. 155–163, https://doi.org/10.1007/978-3-030-47721-9_19.
- [6] G. Sternharz, C. Mares, T. Kalganova, Performance of order-based modal analysis for operational rotating hardware considering excitations composed of various harmonic and random amplitudes, in: *Proceedings of ISMA 2020 - International Conference on Noise and Vibration Engineering*, 2020, pp. 1465–1479.
- [7] K. Janssens, Z. Kollar, B. Peeters, S. Pauwels, H., Van der Auweraer, Order-based resonance identification using operational PolyMAX, in: *Proceedings of the International Modal Analysis Conference (IMAC)*, 2006, pp. 566–575.
- [8] E. Di Lorenzo, S. Manzato, F. Vanhollenbeke, S. Goris, B. Peeters, W. Desmet, F. Marulo, Dynamic characterization of wind turbine gearboxes using Order-Based Modal Analysis, in: *Proceedings of the International Conference on Noise and Vibration Engineering (ISMA)*, 2014, pp. 4349–4362.
- [9] E. Di Lorenzo, S. Manzato, B. Peeters, F. Marulo, W. Desmet, Best Practices for Using Order-Based Modal Analysis for Industrial Applications, in: *Proceedings of the 35th IMAC: Topics in Modal Analysis & Testing*, 2017, pp. 69–84, https://doi.org/10.1007/978-3-319-54810-4_9.
- [10] B. Peeters, P. Gajdatsy, P. Aarnoutse, K. Janssens, W. Desmet, Vibro-acoustic operational modal analysis using engine run-up data, in: *Proceedings of the 3rd International Operational Modal Analysis Conference (IOMAC)*, 2009, pp. 447–455.
- [11] A. Mbarek, A.F. Del Rincon, A. Hammami, M. Iglesias, F. Chaari, F. Viadero, M. Haddar, Comparison of experimental and operational modal analysis on a back to back planetary gear, *Mech. Mach. Theory* 124 (2018) 226–247, <https://doi.org/10.1016/j.mechmachtheory.2018.03.005>.
- [12] E. Di Lorenzo, S. Manzato, B. Peeters, F. Vanhollenbeke, W. Desmet, F. Marulo, Order-Based Modal Analysis: A modal parameter estimation technique for rotating machineries. *Proceedings of the 6th International Operational Modal Analysis Conference (IOMAC)*, 2015.
- [13] P. Vacher, B. Jacquier, A. Bucharles, Extensions of the MAC criterion to complex modes, in: *Proceedings of ISMA 2010 - International Conference on Noise and Vibration Engineering*, 2010, pp. 2713–2725.
- [14] D.F. Aldridge, *Mathematics of Linear Sweeps*, *Can. J. Explor. Geophys.* 28 (1992) 62–68.
- [15] H. Vold, K. Napolitano, D. Hensley, M. Richardson, Aliasing in modal parameter estimation, *Sound Vib.* (2008) 12–17. <http://www.sandv.com/downloads/0801vold.pdf>.
- [16] M.H. Richardson, D.L. Formenti, Parameter estimation from frequency response measurements using rational fraction polynomials, in: *Proceedings of the International Modal Analysis Conference (IMAC)*, 1982, pp. 167–181.
- [17] H.I. Vold, Methods and apparatus for modal parameter estimation, US 2009/0204355 A1, 2009. <https://patents.google.com/patent/US20090204355A1>.
- [18] E. Di Lorenzo, S. Manzato, B. Peeters, F. Marulo, W. Desmet, Operational Modal Analysis for Rotating Machines: Challenges and Solutions. *Proceedings of the 7th International Operational Modal Analysis Conference (IOMAC)*, 2017.
- [19] E. Di Lorenzo, Operational Modal Analysis for Rotating Machines: Challenges and Solutions, Università degli Studi di Napoli Federico II (2017), <https://doi.org/10.6093/UNINA/FEDOA/11469>.
- [20] R.J. Allemang, The modal assurance criterion - Twenty years of use and abuse, *Sound Vib.* 37 (2003) 14–21. <http://sandv.com/downloads/0308alle.pdf>.
- [21] D.J. Ewins, *Modal Testing: Theory, Practice and Application*, 2nd ed., Research Studies Press Ltd., Baldock, Hertfordshire, England, 2000.
- [22] C. Rainieri, G. Fabbrocino, in: *Operational Modal Analysis of Civil Engineering Structures: An Introduction and Guide for Applications*, Springer, 2014, <https://doi.org/10.1007/978-1-4939-0767-0>.
- [23] X. Zhang, L. Yue, Order Based Modal Analysis Using Vold-Kalman Filter, in: *Prognostics and System Health Management Conference*, 2019, <https://doi.org/10.1109/PHM-Qingdao46334.2019.8942927>.
- [24] S. Manzato, E. Di Lorenzo, A. Medici, F. Vanhollenbeke, B. Peeters, W. Desmet, Order Based Modal Analysis Versus Standard Techniques to Extract Modal Parameters of Operational Wind Turbine Gearboxes, in: *Proceedings of the 33rd IMAC: Topics in Modal Analysis*, 2015, pp. 115–122, <https://doi.org/10.1007/978-3-319-15251-6>.
- [25] R. Markert, M. Seidler, Analytically based estimation of the maximum amplitude during passage through resonance, *Int. J. Solids Struct.* 38 (2001) 1975–1992, [https://doi.org/10.1016/S0020-7683\(00\)00147-5](https://doi.org/10.1016/S0020-7683(00)00147-5).
- [26] H.P. Hackenberg, A. Hartung, An Approach for Estimating the Effect of Transient Sweep Through a Resonance, *J. Eng. Gas Turbines Power* 138 (2016) 1–12, <https://doi.org/10.1115/1.4032664>.

- [27] G. Gloth, M. Sinapius, Analysis of swept-sine runs during modal identification, *Mech. Syst. Sig. Process.* 18 (2004) 1421–1441, [https://doi.org/10.1016/S0888-3270\(03\)00087-6](https://doi.org/10.1016/S0888-3270(03)00087-6).
- [28] O. Matsushita, M. Tanaka, H. Kanki, M. Kobayashi, P. Keogh, *Vibrations of Rotating Machinery*, Springer Japan, Tokyo (2017), <https://doi.org/10.1007/978-4-431-55456-1>.
- [29] J.R. Blough, *Improving the Analysis of Operating Data on Rotating Automotive Components*, University of Cincinnati, 1998.
- [30] A. Cattaneo, S. Manzoni, M. Vanali, Frequency resolution and number of averages effects on the accuracy and dispersion of operational modal analysis results, in: *4th International Operational Modal Analysis Conference (IOMAC)*, 2011, pp. 462–472.